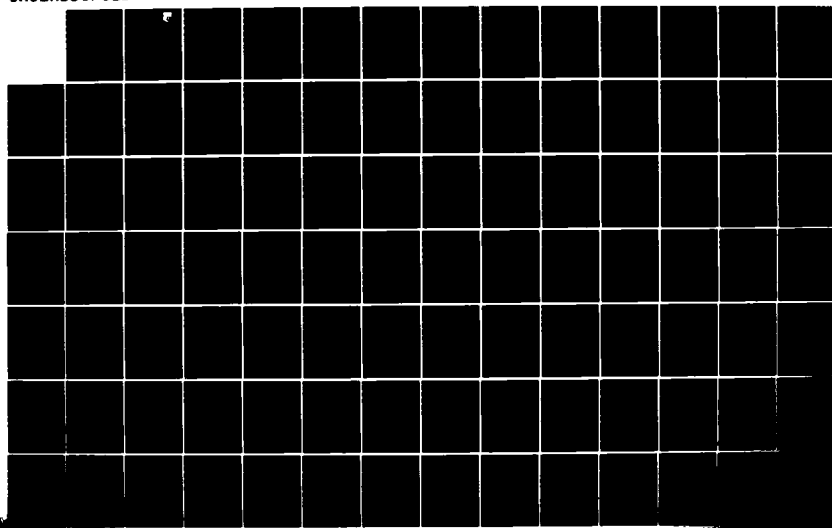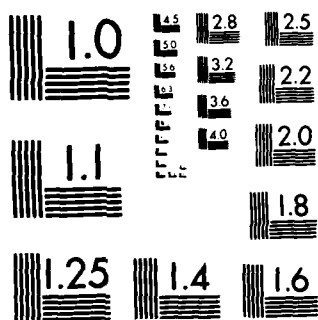MAGNETOSTATIC-WAVE PROPAGATION IN A FINITE YIG-LOADED
RECTANGULAR WAVEGUI..(U) MICHIGAN UNIV ANN ARBOR
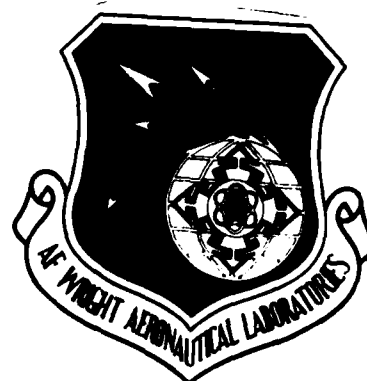SOLID-STATE ELECTRONICS LAB M RADMANESH NOV 84 TR-170

MICROCOPY RESOLUTION TEST CHART
NATIONAL BUREAU OF STANDARDS 1963 A

AD-A150 332

⑫

AFWAL-TR-84-1174

MAGNETOSTATIC-WAVE PROPAGATION IN A FINITE YIG-LOADED RECTANGULAR
WAVEGUIDE

M. Radmanesh

Solid-State Electronics Laboratory
Department of Electrical Engineering and Computer Science
The University of Michigan
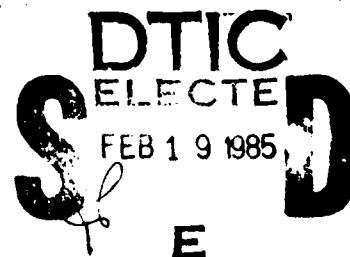Ann Arbor, Michigan 48109

November 1984

Interim Report for Period October 1, 1981-June 30, 1984

Approved for public release; distribution unlimited.

DTIC FILE COPY

DTIC
ELECTE
FEB 1 9 1985
E

85 02 04 030

NOTICE

When Government drawings, specifications, or other data are used
for any purpose other than in connection with a definitely related
Government procurement operation, the United States Government thereby
incurs no responsibility nor any obligation whatsoever; and the fact that
the government may have formulated, furnished, or in any way supplied the
said drawings, specifications, or other data, is not to be regarded by
implication or otherwise as in any manner licensing the holder or any
other person or corporation, or conveying any rights or permission to
manufacture use, or sell any patented invention that may in any way be
related thereto.

This report has been reviewed by the Office of Public Affairs
(ASD/PA) and is releasable to the National Technical Information Service
(NTIS). At NTIS, it will be available to the general public, including
foreign nations.

This technical report has been reviewed and is approved for
publication.

MR. ROBERT BLUMGOLD
Project Engineer
Microwave Techniques &
  Applications Gp

ROBERT T. KEMERLEY, Acting Chief
Microwave Techniques and
  Applications Grp
Microwave Technology Branch

FOR THE COMMANDER

DONALD S. REES, Chief
Microwave Technology Branch
Avionics Laboratory

REPORT DOCUMENTATION PAGE	READ INSTRUCTIONS BEFORE COMPLETING FORM	
1. REPORT NUMBER AFWAL-TR-84-1174	2. GOVT ACCESSION NO. AD-A150332	3. RECIPIENT'S CATALOG NUMBER
4. TITLE (and Subtitle) MAGNETOSTATIC-WAVE PROPAGATION IN A FINITE YIG-LOADED RECTANGULAR WAVEGUIDE		5. TYPE OF REPORT & PERIOD COVERED Interim Tech October 1, 1981–June 30, 1984
		6. PERFORMING ORG. REPORT NUMBER Tech. Report No. 170
7. AUTHOR(s) M. Radmanesh		8. CONTRACT OR GRANT NUMBER(s) F33615-81-K-1429
9. PERFORMING ORGANIZATION NAME AND ADDRESS Solid-State Electronics Laboratory The University of Michigan Ann Arbor, MI 48109		10. PROGRAM ELEMENT, PROJECT, TASK AREA & WORK UNIT NUMBERS 20020392
11. CONTROLLING OFFICE NAME AND ADDRESS Avionics Laboratory (AFWAL/AADM-2) Air Force Wright Aeronautical Laboratories Wright-Patterson AFB, OH 45433		12. REPORT DATE November 1984
		13. NUMBER OF PAGES 160
14. MONITORING AGENCY NAME & ADDRESS(if different from Controlling Office)		15. SECURITY CLASS. (of this report) Unclassified
		15a. DECLASSIFICATION DOWNGRADING SCHEDULE N/A

16. DISTRIBUTION STATEMENT (of this Report)

Approved for public release; distribution unlimited.

17. DISTRIBUTION STATEMENT (of the abstract entered in Block 20, if different from Report)

18. SUPPLEMENTARY NOTES

The findings in this report are not to be construed as an official Department of the Air Force position, unless so designated by other authorized documents.

19. KEY WORDS (Continue on reverse side if necessary and identify by block number)

Magnetostatic-wave propagation
Rectangular waveguide
YIG slab
Magnetostatic-wave devices

20. ABSTRACT (Continue on reverse side if necessary and identify by block number)

The objective of this investigation is to study magnetostatic-wave propagation in a rectangular waveguide loaded with a finite YIG slab, to understand the effect of physical parameters on the dispersion and group time-delay character- istics, and to obtain better design criteria for magnetostatic-wave devices.

An analysis was carried out for two basic geometrical configurations: (1) a YIG slab of arbitrary thickness placed inside a waveguide in contact with each sidewall and (2) a thin YIG slab of finite width placed symmetrically inside a

DD 1 JAN 73 1473

20.

waveguide such that there is an equal air gap between the slab and each sidewall. For each of these basic geometries, the magnetic bias field was assumed to be either parallel or normal to the slab in the transverse plane of the waveguide. For Case 1, the mode analysis technique was used to obtain the dispersion relations while in Case 2 the integral equation method was used to derive the approximate dispersion relations.

Numerical simulations were carried out for various geometrical configurations. Sample numerical calculations of the propagation constant and delay characteristics are presented in the frequency range of 4 to 10 GHz. These numerical results were obtained as a function of the geometry and magnetic field. The results obtained from the numerical simulation will be important in the design of magnetostatic-wave devices.

The general formulation presented in this study contains all the information given by the degenerate cases previously published. *The special cases of interest are obtained simply by permitting some of the dimensional parameters to take on their limiting values.*

FOREWORD

This report describes magnetostatic-wave propagation in a finite YIG-loaded rectangular waveguide. This research was carried out at the Solid-State Electronics Laboratory, Department of Electrical Engineering and Computer Science, The University of Michigan, Ann Arbor, Michigan. The work was sponsored by the Air Force Systems Command, Avionics Laboratory, Wright-Patterson Air Force Base, Ohio under Contract No. F33615-81-K-1429.

The work reported herein was performed during the period October 1, 1981 to June 30, 1984 by Dr. Massoude Radmanesh. The report was released by the author in June 1984.

The author wishes to thank Professors C-M. Chu and G. I. Haddad, his dissertation co-chairmen, for their encouragement, guidance and support and to Professors E. N. Leith, L. R. Scott, and T.B.A. Senior for their helpful discussions and suggestions. He is also grateful to Messrs. A. Vadhidi-Molavi and C-K. Pao for their assistance in this investigation.

Accession For		
NTIS GRA&I	☒	
DTIC TAB	☐	
Unannounced	☐	
Justification		
By		
Distribution/		
Availability Codes		
	Avail and/or	
Dist	Special	
A-1		

DTIC
COPY
INSPECTED
9

iii

TABLE OF CONTENTS

v

LIST OF ILLUSTRATIONS

LIST OF TABLES

x

LIST OF SYMBOLS

a	Waveguide width.
$\overline{B}$	Total magnetic flux density vector.
b	Waveguide height.
$\overline{b}$	RF portion of $\overline{B}$ field.
D	Value of the determinant.
$D_N(f,K)$	Determinant of the N x N truncated matrix.
d	One half slab thickness.
$\overline{e}$	RF electric field vector.
$f_0(x), f_1(x), f_2(x)$	Potential functions defined at $z = z_0$, z_1 and z_2, respectively.
G	Green's function.
G_1, G_2	Green's function defined in the regions below and above the source point, respectively.
$G_s(x), G_v(x)$	Functions constructed from $f_0(x)$, $f_1(x)$ and $f_2(x)$.
$\overline{H}$	Total internal magnetic field.
$[H]$	$(2N_0 + 1) \times (2N_0 + 1)$ coefficient matrix for the normal magnetization case.
$\overline{H}_0$	Internal dc magnetic field.
$\overline{H}_{dc}$	Applied dc magnetic field.
$\overline{h}$	RF portion of $\overline{H}$ field.
$\overline{\overline{I}}$	Identity tensor.
I_{s_1}, I_{s_2}	Surface integral expressions.
I_{v_1}, I_{v_2}	Volume integral expressions.
j	Pure imaginary number.
K	Wave number in a ferrite material.

K_o	Wave number in free space.
ℓ	Lattice constant of the ferrite.
$\overline{M}$	Total magnetic moment vector per unit volume.
M_o	Saturation magnetization.
M_{ij}	A 2 x 2 matrix involved in determinant calculations.
$\overline{m}$	RF portion of $\overline{M}$.
m_x, m_y, m_z	The three components of vector $\overline{m}$.
N	Size of the truncated matrix.
N_o	A very large integer number.
$\hat{n}$	Unit vector normal to the slab surface.
Q^n	An expression involving $G_s(x)$ and $G_v(x)$.
$\overline{r}$	Position vector to the observation point.
s_1, s_2	Thickness of the bottom and the top air regions, respectively.
t	Time.
t	Slab thickness.
U^n, V_n, W^n	Constants whose values depend on the device dimensions.
x	Horizontal coordinate, abscissa.
x_o	Gap length.
z	Vertical coordinate, latitude.
z_o	Position of the slab center-line.
z_1, z_2	Position of the bottom and top slab interfaces, respectively.
α_n	Phase constant in the x-direction in YIG for normal magnetization.
γ	Gyromagnetic ratio, equal to 1.759×10^{11} C/kg.
γ_n, γ'_n	Phase constant in the z-direction in YIG for parallel and normal magnetization, respectively.
γ'_n	Phase constant in the z-direction in the air regions.

δ_{on}	Kronecker delta function.
ε	Dielectric permittivity.
θ	Angle between the z-axis and the propagation vector in the y-z plane.
θ_o	Angle between the YIG-slab plane and the bias magnetic field vector applied in the transverse plane.
$\bar{\bar{\mu}}$	Magnetic permeability tensor.
μ_o	Magnetic permeability of free space.
$\bar{\bar{\mu}}_r$	Relative magnetic permeability tensor.
ρ_m	Total fictitious magnetic charge density.
ρ_s	Magnetic surface charge density.
ρ_{s_1}, ρ_{s_2}	Magnetic surface charge densities at $z = z_1$ and z_2, respectively.
ρ_v	Magnetic volume charge density.
σ	Electrical conductivity.
τ_d	Group time delay per unit length.
ϕ	Scalar magnetic potential.
$\tilde{\phi}$	Potential in the YIG region $x_o \leqq x \leqq a - x_o$, $z_1 \leqq z \leqq z_2$ (integral equation).
ϕ_1, ϕ_3	Potential functions in the top and bottom air regions, respectively.
ϕ_2	Potential function in the YIG region (mode analysis).
ω	Operating frequency.
ω_o	Natural precession frequency.
ω_{ex}	Exchange frequency.
ω_M	Magnetization-saturation frequency.
ω_r	Modified natural precession frequency.

CHAPTER I. INTRODUCTION

1.1 Magnetostatic-Wave (MSW) Devices

The purpose of this work is to study magnetostatic-wave
propagation in a rectangular waveguide partially filled with a
lowloss ferrite material. The dispersion relation and group time
delay characteristics of the waves are investigated.

Magnetostatic waves are slow dispersive magnetically domi-
nated spin waves that propagate in magnetically biased ferrite slabs
at microwave frequencies. The most common lowloss ferrite material
used for MSW propagation is epitaxial yittrium iron garnet (YIG).

The recent interest in MSW devices at microwave frequencies
has accelerated because the growth of uniform, high-quality, low-
loss epitaxial YIG films with a large aspect ratio has been improved
and the design and fabrication of efficient RF to MSW transducers
have been developed and realized.[1] The first development provides
a uniform internal dc magnetic bias field so that many inhomogeneous
transmission problems associated with nonuniform internal fields are
eliminated. The second development reduces coupling losses from RF
waves to magnetostatic waves so that the overall insertion loss
can be reduced greatly. Another motivation for exploring the use
of magnetostatic waves in microwave signal processing is due to
the fact that MSW operation is possible in the frequency range of
1.0 to 20.0 GHz with wide instantaneous bandwidths in contrast to
conventional devices such as surface-acoustic-wave (SAW) devices
which usually operate on the IF signal.

A comparison of the relative merits of MSW devices and SAW devices is given by Owens et al.[2] and Collins et al.[3] and is presented in Table 1.1. From this table it can be seen that the tunable properties, the lower propagation losses at microwave frequencies, the invariant transducer geometry, and the adjustable delay properties of magnetostatic-wave devices present a major advantage in terms of device performance over other existing devices such as SAW devices.

Table 1.1

Characteristic Features of MSW and SAW Devices[2,3]

Property	MSW	SAW
Maximum delay per cm	Hundreds of ns	Hundreds of μs
Transducer geometry	Simple/moderately complex	Complex
Transducer dimensions	Invariant with frequency	Decrease as frequency increases
Bandpass filtering capability	Good	Excellent
Adjustable delay	Yes	Not in a single device
Power handling	1 mW	1 W
Typical velocity (km/s)	10 to 1000	2 to 6
Typical attenuation (dB/μs)	5 at 1 GHz; 20 at 10 GHz	1 at 1 GHz; 60 at 10 GHz
Dispersion	Yes	No

Based on recent literature,[4-9] the possible applications of MSW devices are summarized in Table 1.2. From this table, it can be seen that MSW devices cover a wide range of applications in

Table 1.2

Prime Applications of MSW Devices

Device	Microwave Function
Nondispersive delay line	Phase locking of pulsed oscillator, signal correlation, communication path length equalizer, rate sensor
Dispersive delay line	Group delay equalizer, pulse compression, compressive receiver, rate sensor, frequency synthesis
Tapped delay line	ECM deception, PSK matched filter, Fourier transformation
Variable delay line	Target simulation, electronic timing
Bandpass filter	ECM, radar, communication satellite repeaters
Tunable resonator	Narrow-band frequency filter and oscillator applications
MSW directional coupler	Signal routing, switched delay line
MSW oscillator	Stable microwave source

microwave communication systems. As noted in this table, their prime applications are in the areas of delay lines, filters, oscillators, and resonators.[10-19] The conventional means of exciting magnetostatic waves are by metal transducers that have been analyzed extensively in the literature.[20-35]

1.2 Previous Investigations.

Previous analyses of various types of geometries for MSW propagation have included the following:

1. The first structure consisted of a YIG film deposited on a substrate (see Fig. 1.1) and was investigated by Damon and Eshback.[36] The input and output transducers were microstrip lines. They determined the different propagating modes that can exist in this structure. A summary of all the propagating modes for different magnetization directions was reported by Adams et al.[9]

2. A multilayer planar structure with ground planes was considered by Tsai et al.[37] and others[38,39] (see Fig. 1.2). In this work, wave propagation in a normally magnetized structure of infinite width was analyzed. Daniel et al.[40] reported a complete summary of the wave propagation in this structure for principal directions of magnetization.

3. Young[41] considered wave propagation in a metallic trough partially filled with YIG material as shown in Fig. 1.3. He derived the dispersion relation for two important propagating modes that can exist when magnetization is parallel to the slab plane.

4. Finally, a long rectangular YIG rod with metal boundaries was investigated by Auld and Mehta[42] (see Fig. 1.4). They studied

FIG. 1.1 YIG SLAB IN FREE SPACE.

$$\sigma \longrightarrow \infty$$

YIG

s_1

t

s_2

z

x

$\bar{H}_{dc}$

$$\sigma \longrightarrow \infty$$

FIG. 1.2 YIG SLAB BETWEEN TWO GROUND PLANES.

FIG. 1.- YIG SLAB IN A METALLIC TROUGH.

FIG. 1.4   COMPLETELY FILLED GUIDE.

two possible modes of propagation in this structure, using a mode analysis technique, and derived a dispersion relation for each case.

It is to be noted that in all the reported structures, the ferrite is inside an unbounded space except when the guide is completely filled. The case of a ferrite slab enclosed in a waveguide as shown in Fig. 1.5 has never been studied. This study will concentrate on the analysis of this general structure.

1.3 Outline of the Present Study

The purpose of this study is to analyze magnetostatic-wave propagation in YIG slabs placed inside a rectangular waveguide as illustrated in Fig. 1.5. The general formulation of the equations for magnetostatic-wave propagation and some known results for certain special structures are given in Chapter II.

In Chapter III, the case of a ferrite slab in contact with both sidewalls of the waveguide is discussed. This part can be treated as a boundary value problem and the method of mode analysis is conveniently applied. In this method a certain mathematical form for the potential function in each region is adopted so that it satisfies the boundary conditions. Matching the potential fields and normal field components at the slab interfaces gives a system of linear equations which, upon mathematical manipulation, yields the desired dispersion relation.

When the width of the slab is less than the width of the guide, that is, when $x_o \neq 0$ (Fig. 1.5), the mode analysis appears to be fruitless and the integral equation seems to be more appropriate. For simplicity, the slab is assumed to be thin ($t \rightarrow 0$) and

FIG. 1.5   DEVICE CONFIGURATION.

mathematically it represents the source of magnetic charges. In this way the integral equation is tractable and yields the dispersion relations. This is given in Chapter IV. Parallel and normal magnetization are considered separately in the wave analysis of Chapters III and IV.

In Chapter V, numerical methods employed in obtaining numerical data and dispersion plots are presented. The results presented in this chapter extensively describe the device behavior and performance under different geometrical configurations.

Finally, Chapter VI summarizes this study, sets out conclusions, and offers suggestions for further study. Appendix A contains sample computer programs developed to investigate the structure shown in Fig. 1.5 for $\overline{H}_{dc}$ in the x- and z-directions.

CHAPTER II. MAGNETOSTATIC-WAVE PROPAGATION

2.1 Introduction

In this chapter, the mathematical foundation for magnetostatic-wave propagation in unbounded and bounded ferrite media is introduced and the governing equations are derived. With the help of a permeability tensor derived for an anisotropic magnetic medium, it is shown that plane wave propagation of electromagnetic waves in unbounded ferrites leads to three regions of interest in the frequency (ω)-wave number (K) plane. It is seen that magnetostatic-wave propagation is possible only in a limited range of wavelengths. In this range of wavelengths, Maxwell's equations can be simplified which makes it possible to ignore the electric field and derive the magnetic field directly from a scalar potential field. When this approximation is used, the governing partial differential equations inside the YIG slab can be derived.

Wave propagation in a loaded rectangular waveguide under the magnetostatic approximation is discussed and a set of boundary conditions which must be satisfied at the metal surfaces and slab interfaces are introduced. Finally, some known structures are analyzed and the results are presented.

2.2 Derivation of Effective Permeability.

Ferrites are ceramic-like magnetic materials whose high resistivity makes eddy current losses extremely low at microwave frequencies. The tensor permeability of a ferrite is derived using Newton's equation of motion where the exchange

forces and core losses are neglected:[42-45]

$$\frac{d\overline{M}}{dt} = \gamma \mu_o (\overline{M} \times \overline{H}) \quad , \tag{2.1}$$

where $\overline{M}$ = the total magnetic moment per unit volume,

$\overline{H}$ = the total internal magnetic field and

γ = the gyromagnetic ratio which is equal to 2.8 MHz/Oe, in Cgs system.

Assuming harmonic time dependence Eq. 2.1 may be expressed as follows:

$$\frac{d}{dt}(\overline{M}_o + \overline{m}e^{j\omega t}) = \gamma \mu_o (\overline{M}_o + \overline{m}e^{j\omega t}) \times (\overline{H}_o + \overline{h}e^{j\omega t})] \quad , \tag{2.2}$$

where $\overline{M}_o$ is the saturation magnetization vector; $\overline{H}_o$ is the dc magnetic field vector inside the slab which, due to the neglect of demagnetization fields, is the same as that outside the slab;[46,47] and $\overline{m}$ and $\overline{h}$ are the RF magnetic moment per unit volume and the RF magnetic field intensity vectors, respectively.

Assuming the dc fields are much larger than the RF fields and neglecting the terms of order higher than the first, Eq. 2.2 becomes:

$$j\omega\overline{m} = \mu_o \gamma (\overline{M}_o \times \overline{h} + \overline{m} \times \overline{H}_o) \quad . \tag{2.3}$$

If $\overline{H}_o$ is in the z-direction and $\overline{h}$ is perpendicular to $\overline{H}_o$, then Eq. 2.3 can be expressed in terms of its components as follows:

$$m_x = \mu_o(\chi h_x - j\kappa h_y) \quad ,$$

$$m_y = \mu_o(j\kappa h_x + \chi h_y)$$

and

$$m_z = 0 \quad ,$$

where

$$\chi = \omega_m \omega_o / (\omega_o^2 - \omega^2) \quad ,$$

$$K_1 = \omega\omega_M/(\omega_o^2 - \omega^2) \quad ,$$

$$\omega_o = \mu_o\gamma H_o$$

and

$$\omega_M = \mu_o\gamma M_o \quad .$$

Expressing these results in terms of a permeability tensor yields

$$\overline{b} = \mu_o(\overline{h} + \overline{m}) = \overline{\overline{\mu}} \cdot \overline{h} \quad ,$$

where

$$\overline{\overline{\mu}} = \mu_o\overline{\overline{\mu}}_r$$

and $\overline{\overline{\mu}}_r$ is the relative permeability tensor and is given by[48]

$$\overline{\overline{\mu}}_r = \begin{bmatrix} \mu & jK_1 & 0 \\ -jK_1 & \mu & 0 \\ 0 & 0 & 1 \end{bmatrix} \quad , \tag{2.4a}$$

where $\mu = 1 + \chi$. If H_o is in the x-direction, $\overline{\overline{\mu}}_r$ from Eq. 2.4a

becomes

$$\overline{\overline{\mu}}_r = \begin{bmatrix} 1 & 0 & 0 \\ 0 & \mu & jK_1 \\ 0 & -jK_1 & \mu \end{bmatrix} \quad . \tag{2.4b}$$

The relative permeability tensor given by Eqs. 2.4 is the value of

effective permeability that must be used in Maxwell's equation for

regions containing ferrites. In order to include the effect of

exchange forces, ω_o in Eq. 2.4 must be replaced simply by[48]

$\omega_r = \omega_o + \omega_{ex}\ell^2 K_o^2$ where $\omega_{ex} = \gamma H_{ex}$, ℓ and K_o are the lattice constant

and the free-space wave number, respectively, and H_{ex} is the internal

exchange field. Maxwell's equation in conjunction with the permeability

tensor from Eqs. 2.4 can be used to study plane-wave propagation in

unbounded ferrite media.

2.3 Plane Wave Propagation in Unbounded Ferrites

Magnetostatic waves have wavelengths much greater than the

lattice spacing and therefore it is appropriate to use classical

theory rather than quantum theory. The small-signal theory of a

lossless ferrite is based on Maxwell's equations. They can be

written[49,50] in a form that includes the permeability tensor of the

ferrite. A plane wave solution of the form $e^{j(\omega t - \overline{K} \cdot \overline{r})}$ is assumed.

It therefore follows that:

$$\nabla \times \overline{h} = j\omega \varepsilon \overline{e} \ ,$$

$$\nabla \times \overline{e} = -j\omega \mu_0 \overline{\overline{\mu}} \cdot \overline{h} \ , \qquad (2.5)$$

$$\nabla \cdot \varepsilon \overline{e} = 0$$

and

$$\nabla \cdot (\overline{\overline{\mu}} \cdot \overline{h}) = 0 \ .$$

Solutions to Eq. 2.5 were discussed by Seidel.[51] It is con-

venient to assume that the magnetic bias field is in the z-direction

and the propagation vector is in the y-z plane at an angle θ with

the z axis. Including the exchange term in the permeability tensor,

the dispersion relation is found to be:

$$\frac{K^2}{K_o^2} = \frac{(\mu^2 - \mu - K_1^2) \sin^2 \theta + 2\mu \pm [(\mu^2 - \mu - K_1^2) \sin^4 \theta + 4K_1^2 \cos^2 \theta]^{\frac{1}{2}}}{2[(\mu - 1) \sin^2 \theta + 1]}$$

$$, \quad (2.6)$$

where $K_o^2 = \omega^2 \epsilon \mu_o$. The corresponding RF electric and magnetic fields are:

$$\bar{e} = -\frac{K_o}{K}\left(\frac{\mu_o}{\epsilon}\right)^{\frac{1}{2}} \begin{bmatrix} j \dfrac{\mu(K_o/K)^2 - 1}{K_1} \cdot \dfrac{\cos\theta}{\sin^2\theta - (K_o/K)^2} \\ \cos\theta \\ -\sin\theta \end{bmatrix} e^{-j\bar{K}\cdot\bar{r}} \quad (2.7)$$

and

$$\bar{h} = \begin{bmatrix} (K_o/K)^2 \\ j \dfrac{\mu(K_o/K)^2 - 1}{K_1} \\ j \dfrac{\mu(K_o/K)^2 - 1}{K_1} \cdot \dfrac{\cos\theta \sin\theta}{\sin^2\theta - (K_o/K)^2} \end{bmatrix} e^{-j\bar{K}\cdot\bar{r}} \quad . \quad (2.8)$$

Equation 2.6 defines a manifold of dispersion curves[56] bounded by curves $\theta = 0$ degrees and $\theta = 90$ degrees as shown in Fig. 2.1. At each value of θ the medium supports two types of waves, an ordinary wave for which $K/K_o \cong 1$ and an extraordinary wave for which K/K_o becomes very large at certain frequencies. As seen in Fig. 2.1, the inclusion of exchange forces causes the lower branches of the extraordinary curves to bend upward for large values of K/K_o.

The lower branches in Fig. 2.1 may be divided conveniently into three regions.

1. $K/K_o \cong 1$. Here the electric and magnetic fields of Eqs. 2.7 and 2.8 are of comparable magnitude. This may be termed the region of "electromagnetic propagation."

OPERATING FREQUENCY ω, GHz

ORDINARY WAVE

EXTRAORDINARY WAVE

$\theta = 90°$

$\theta = 0$

$K = K_0$

$\theta = 0$

$\theta = 90°$

CHANGE OF SCALE

WAVE NUMBER K, cm^{-1}

I   II   III

$\omega_0 + \omega_M$

$(\omega_0^2 + \omega_M \omega_0)^{1/2}$

ω_0

FIG. 2.1 OPERATING FREQUENCY IN THE INFINITE MEDIUM AS A FUNCTION OF WAVE NUMBER, WHERE K = 0 CORRESPONDS TO THE FREQUENCY OF UNIFORM PRECESSION. THE REGIONS INDICATED ARE (I) ELECTROMAGNETIC PROPAGATION, (II) MAGNETOSTATIC MODES, AND (III) SPIN-WAVE MODES. THIS FIGURE IS DRAWN FOR $H_o = M_o = 2000$ Oe. (LAX AND BUTTON[50])

2. $1 \ll K/K_o \ll \omega_o/(\omega_{ex}\ell^2 K_o^2)$. From Eq. 2.7 it is seen that the electric field is negligibly small in this region compared with the magnetic field and can eventually be neglected. Equation 2.8 becomes:

$$\overline{h} = \begin{bmatrix} 0 \\ -j/K_1 \\ -j \cot \theta/K_1 \end{bmatrix} e^{-j\overline{K}\cdot\overline{r}} , \qquad (2.9)$$

where terms of order $(K_o/K)^2$ have been neglected. It is shown easily that the magnetic field in Eq. 2.9 satisfies the magnetostatic equations which can be derived from Eq. 2.5 as follows:

$$\nabla \times \overline{h} = 0 \qquad (2.10a)$$

and

$$\nabla \cdot (\overline{\overline{\mu}} \cdot \overline{h}) = 0 . \qquad (2.10b)$$

This may, therefore, be termed the region of "magnetic propagation." It corresponds to the very flat portions of the dispersion curves where the frequency is $\omega^2 = \omega_o(\omega_o + \omega_M \sin^2 \theta)$. These waves are, therefore, characterized by a low-phase velocity and a negligibly small group velocity.

3. $\omega_o/(\omega_{ex}\ell^2 K_o^2) \ll K/K_o$. Here the magnetic field is again given by Eq. 2.9. However, the exchange term now has a significant effect on the shape of the dispersion curves which bend upward into the familiar exchange spin-wave manifold:

$$\omega^2 = (\omega_o + \omega_{ex}\ell^2 K^2)(\omega_o + \omega_{ex}\ell^2 K^2 + \omega_M \sin^2 \theta) .$$

This may be termed the region of "exchange propagation." These

regions are of course not sharply defined, since the propagation
characteristics vary continuously with K/K_o.

The wave propagation discussed here was in the absence of any
surfaces and basically ignored the finite dimensions of the ferrite
material which is of significant value to engineering problems. Most
of the structures studied so far in the literature are slabs of
finite thickness and infinite width. In the next section the
governing equations for magnetostatic-wave propagation are derived
and the boundary conditions that must be satisfied by the propagating
waves are given. Finite dimensions of the ferrite material and the
relative orientation of the magnetic bias field with respect to the
propagation vector $\bar{K}$ lead to different modes of propagation which are
discussed in the next section.

2.4 Magnetostatic-Wave Propagation

Wave propagation in a ferrite medium of infinite extent was
considered in the previous section. The validity of this idealization
as an approximation to the magnetostatic-wave propagation in a finite
medium of a rectangular waveguide is examined next (see Fig. 1.5).[52-54]
The transverse dimensions of the waveguide are small compared to the
electromagnetic wavelength and the electromagnetic modes are either
cut-off waves or leaky waves.

2.4.1 Governing Equations. In Section 2.3 it was shown that
Maxwell's equations in the magnetostatic approximation reduce to:

$$\nabla \times \bar{H} = 0 \tag{2.11a}$$

and

$$\nabla \cdot (\mu \cdot \bar{H}) = 0 . \tag{2.11b}$$

This permits the definition of a magnetic scalar potential ϕ by defining $\overline{h} = \nabla\phi$. The magnetostatic field inside the ferrite is governed by the equation:

$$\nabla \cdot \overline{\overline{\mu}}\nabla\phi = 0 \quad . \tag{2.12}$$

When H_{dc} is either in the x- or z-direction, Eq. 2.12 takes the following forms:

$$\phi_{zz} + \mu(\phi_{xx} + \phi_{yy}) = 0 \quad , \quad H_{dc} \parallel \hat{z} \tag{2.13a}$$

and

$$\phi_{xx} + \mu(\phi_{zz} + \phi_{yy}) = 0 \quad , \quad H_{dc} \parallel \hat{x} \quad . \tag{2.13b}$$

The scalar magnetic potential satisfies the following equation:

$$\nabla^2\phi = 0$$

or

$$\phi_{xx} + \phi_{yy} + \phi_{zz} = 0 \tag{2.13c}$$

outside the ferrite.

In all succeeding analyses, the time harmonic variation $e^{j\omega t}$ is assumed and is omitted for simplicity. The wave propagation is in the y-direction and varies as e^{-jKy}. Thus Eqs. 2.13 reduce to the following forms in the YIG slab:

$$\mu\phi_{xx} + \phi_{zz} = \mu K^2\phi \quad , \quad H_{dc} \parallel \hat{z} \quad , \tag{2.14a}$$

$$\phi_{xx} + \mu\phi_{zz} = \mu K^2\phi \quad , \quad H_{dc} \parallel \hat{x} \tag{2.14b}$$

and in air

$$\phi_{xx} + \phi_{zz} = K^2\phi \quad . \tag{2.14c}$$

2.4.2 Boundary Conditions. The YIG slab is enclosed in a metallic waveguide and the following boundary conditions should be satisfied at all metallic guidewalls (see Fig. 1.5):

$$1. \quad t_x = 0 \quad \text{at } x = 0, a \qquad (2.15a)$$

and

$$2. \quad b_z = 0 \quad \text{at } z = 0, t \quad . \qquad (2.15b)$$

As seen in Fig. 1.5, the conditions that must be satisfied at the four slab-air interfaces are as follows:

$$3. \quad \phi \text{ continuous at } z = z_1, z_2 \quad , \qquad (2.16a)$$

$$4. \quad \phi \text{ continuous at } x = x_0, (a - x_0) \quad , \qquad (2.16b)$$

$$5. \quad b_z \text{ continuous at } z = z_1, z_2 \qquad (2.16c)$$

and

$$6. \quad b_x \text{ continuous at } x = x_0, (a - x_0) \quad . \qquad (2.16d)$$

In general, this problem is best solved by the integral equation method where the slab can be considered to be the source of magnetic charges. This formulation, though complex, is very successful when the slab width is less than the guide width and provides accurate answers to the dispersion calculations required for plotting the curves. This general case is discussed and analyzed in Chapter IV. However, in the special case when the YIG slab extends to both guide sidewalls, the problem can be treated as a boundary value problem and a simpler method, i.e., mode analysis, would be very effective in this case. This case is considered in Chapter III.

2.4.3 Modes of Propagation. Magnetostatic-wave propagation in thin films has been investigated extensively and three major propagating modes have been used in device applications.[55-60] These three modes are determined by the relative orientation of the bias magnetic field, propagation direction, and the ferrite slab. These modes are dispersive and characterized by a limited propagation

passband and magnetic bias tunability. The following is a brief discussion of these modes.

1. The magnetostatic-surface-wave (MSSW) mode in which the bias field $\overline{H}_{dc}$ is perpendicular to the direction of wave propagation and both are in the plane of the film. This mode has highly anisotropic propagation in the film plane and the mode energy is confined to the "top" surface for forward propagation and to the "bottom" surface for reverse propagation.

2. A second mode is the magnetostatic-forward-volume wave (MSFVW) in which the bias field $\overline{H}_{dc}$ is perpendicular to the film plane and is characterized by approximately isotropic propagation in the plane of the slab. The lowest-order mode is usually most easily excited.

3. The third mode, the magnetostatic-backward-volume wave (MSBVW) exists when the direction of the bias field and propagation are the same and in the film plane. This mode has opposite phase and group velocity directions, is highly anisotropic, and is multimoded as in the MSFVW case.

Figure 2.2 shows the dispersion characteristics of the three modes of operation propagating only in certain frequency ranges.[9] In this figure the dispersion characteristic of a surface wave when one of the surfaces is metallized is also shown. As can be seen, the propagation bandwidth increases and device performance is now different.

The idea of placing ground planes in the vicinity of a YIG slab and thus changing its dispersive characteristics and its group delay was investigated.[37-40] In the following section, the

FIG. 4.2 DISPERSION CHARACTERISTICS OF MAGNETOSTATIC
WAVES (ADAMS ET AL.[9])

progressive structural development of the device is cited and briefly
analyzed. In most of these investigated structures, the YIG slab is
assumed to have finite thickness and infinite width. The latter
assumption is not realistic in an engineering sense and needs to be
modified. In Chapters III and IV, finite-width slabs are considered
under general boundary conditions.

2.4.4 Results of Previous Investigations. A literature
review of propagating waves in several structures is presented next.

1. Unshielded slab in free space.[9] This configuration is shown
in Fig. 2.3 where three principal directions of magnetic bias fields are
shown. The three different cases are discussed next.

a. $\overline{H}_{dc}$ in the x-direction. The propagating waves in this
case are called magnetostatic-surface waves (MSSW) and the dispersion
relation is given by:[61]

$$e^{2Kt} = \frac{(\omega_M/2)^2}{[\omega_o + (\omega_M/2)]^2 - \omega^2} ,$$

(2.17)

where t = the slab thickness.

b. $\overline{H}_{dc}$ in the y-direction. The propagating waves in this
case are termed magnetostatic-backward-volume waves (MSBVW) and the
dispersion relation is found to be:[62-64]

$$2 \cot \alpha Kt = \alpha - \alpha^{-1} ,$$

(2.18)

where

$$\alpha = \frac{\omega^2 - \omega_o^2}{\omega_o(\omega_o + \omega_M) - \omega^2} .$$

c. $\overline{H}_{dc}$ in the z-direction. These waves are called
magnetostatic-forward-volume waves (MSFVW) and the dispersion
relation is given by:[65,66]

FIG. 2.3 UNSHIELDED FERRITE SLAB IN FREE SPACE. (THE THREE
PRINCIPAL DIRECTIONS OF MAGNETIC BIAS FIELD ARE
SHOWN.)

$$\tan (Kt/2\alpha) = \alpha \quad , \tag{2.19}$$

where

$$\alpha = \frac{\omega^2 - \omega_o^2}{\omega_o(\omega_o + \omega_M) - \omega^2} \quad .$$

The three waves are for a slab extending in width and length to infinity but with a finite thickness. Equations 2.18 and 2.19 provide many modes due to the sinusoidal nature of the dispersion relations.

2. YIG slab between ground planes.[37-39] Two cases of interest are dicussed (see Fig. 1.2):

a. Parallel magnetization. The dispersion relation is given by:[40]

$$e^{2Kt} = \frac{(\mu - K_1 - \tanh Ks_1)(\mu + K_1 - \tanh Ks_2)}{(\mu + K_1 + \tanh Ks_1)(\mu - K_1 + \tanh Ks_2)} \quad . \tag{2.20}$$

b. Normal magnetization. The dispersion relation for this case is found to be:[40]

$$\tan (\alpha Kt) = \frac{\alpha^2(\tanh Kz_2 + \tanh Kz_1)}{\alpha^2 - \tanh K's + \tanh K's} \quad , \tag{2.21}$$

where $\alpha^2 = - \mu, \mu < 0$.

3. Partially shielded slab with parallel magnetization. The geometry for this case is shown in Fig. 2.4. Two modes of propagation are possible in this case and there are discussed below.

a. The first mode arises in the configuration of Fig. 2.4a and is called the ferrite-metal (FM) mode. The surface wave clings to the shielded surface. The dispersion relation is given by[41]

(a) FM MODES

(b) FA MODES

FIG. 2.4   RECTANGULAR COORDINATE SYSTEM FOR A SMALL YIG SLAB MAGNETIZED WITH TRANSVERSE MAGNETIC FIELD. YIG THICKNESS IS ASSUMED TO BE VERY THIN (a<<b).

$$K = (\gamma_n'/2K_1)\{[1 + 4(\mu\gamma_n/\gamma_n')^2 + 4(\mu\gamma_n/\gamma_n') \coth \gamma_n a]^{\frac{1}{2}} - 1\} \quad,$$

$$(2.22)$$

where

$$\gamma_n = \{[(n\pi/b)^2 + \mu K^2]/\mu\}^{\frac{1}{2}} \quad, \quad n = 0,1,2,3,\ldots,$$

and

$$\gamma_n' = [(n\pi/b)^2 + K^2]^{\frac{1}{2}} \quad.$$

b. The second mode arises in the configuration of Fig. 2.4b and is referred to as the ferrite-air (FA) mode. Here the surface wave fields cling to the unshielded surface. The dispersion relation is given by[41]

$$K = (\gamma_n'/2K_1)\{[1 + 4(\mu\gamma_n/\gamma_n')^2 + 4(\mu\gamma_n/\gamma_n') \coth \gamma_n a]^{\frac{1}{2}} + 1\} \quad,$$

$$n = 0,1,2,3,\ldots. \quad (2.23)$$

When the direction of propagation or the magnetic field direction are reversed, the properties of the FA and FM modes are interchanged. These are shown in Fig. 2.5.

4. Completely filled guide.[42,52] The structure for this case is shown in Fig. 2.6a. It is found that the propagating modes are either surface or volume waves that propagate in different frequency ranges.

a. Volume modes. The dispersion relation for this mode is given by $(n,m \neq 0)$

$$K^2 = - (n\pi/b)^2/\mu - (m\pi/a)^2 \quad, \quad \mu < 0 \quad, \quad (2.24)$$

where m,n are nonzero integers.

FIG. DISPERSION CURVES FOR FM AND FA SURFACE WAVES IN A PARTIALLY SHIELDED SLAB.

(a)

(b)

FIG. 2.6 COMPLETELY FILLED GUIDE. THE DISPERSION CURVES ARE
INDEPENDENT OF DIMENSION a.

b. Surface waves. The dispersion relation for this case is given by

$$K^2 = \frac{(n\pi/b)^2}{(K_1^2/\mu) - \mu} \quad , \quad \mu > 0 \quad . \tag{2.25}$$

These two cases are plotted in Fig. 2.6b for H_{dc} = 500 Oe and a = b. In this particular case, the dispersion relation can be shown to be independent of dimension a.[42] As noticed here in almost all the structures, magnetostatic-wave propagation was studied in unbounded media, thus giving only an approximately answer to the problem of the wave propagation in finite-width YIG slabs in the presence of boundary surfaces made of metal. Under these general conditions the solutions offered here by the widely known boundary-value-problem technique would no longer hold and a more powerful technique, i.e., the integral equation method, must be employed in order to obtain reasonable answers.

CHAPTER III. MODE ANALYSIS

3.1 Introduction

In this chapter magnetostatic-wave propagation inside a waveguide partially filled with a YIG slab (see Fig. 3.1) is investigated by the mode analysis technique. The slab extends to both guide sidewalls and therefore the problem can be treated as a boundary value problem.

The differential equations to be solved are:

$$\nabla \cdot (\overline{\overline{\mu}} \nabla \phi) = 0$$

in the YIG and the Laplace equation $\nabla^2 \phi = 0$ in air. The potential field in the air or YIG regions can be written in terms of a Fourier series expansion. The Fourier series expansion in each region should satisfy the boundary conditions at all metal surfaces as given in Section 2.4.2.

Matching the potential functions at the slab interfaces provides a system of linear equations. Rewriting the system of linear equations in matrix form and requiring a nontrivial solution to the problem results in setting the determinant of the coefficient matrix to zero. Solving this equation for roots yields the dispersion characteristics.

3.2 Potential Fields in the Air Region

In Fig. 3.1, the differential equation that should be solved in the air region is the Laplace equation:

$$\phi_{xx} + \phi_{zz} = K^2 \phi \quad . \tag{3.1}$$

FIG. 3.1 WAVEGUIDE PARTIALLY FILLED WITH A YIG SLAB.

Solutions to Eq. 3.1 in the air regions (I and III) can be written
as a combination of even and odd sinusoidal harmonics in the x-
direction and in terms of hyperbolic functions in the z-direction
as follows:

$$\phi_1 = \sum_{n=0}^{\infty} \left[A_{1n} \cos \frac{n\pi}{a} x + B_{1n} \sin \frac{n\pi}{a} x \right] [C_{1n} \sinh \gamma_n'(b - z)$$

$$+ D_{1n} \cosh \gamma_n'(b - z)] \, e^{-jKy} \quad (3.2a)$$

and

$$\phi_3 = \sum_{n=0}^{\infty} \left[A_{3n} \cos \frac{n\pi}{a} x + B_{3n} \sin \frac{n\pi}{a} x \right] [C_{3n} \sinh \gamma_n'(b - z)$$

$$+ D_{3n} \cosh \gamma_n'(b - z)] \, e^{-jKy} \quad , \quad (3.2b)$$

where

$$\gamma_n' = \left[K^2 + \left(\frac{n\pi}{a} \right)^2 \right]^{1/2} \quad .$$

Equations 3.2 should now satisfy the boundary conditions given in
Section 2.4.2. From Condition 1, $E_x = (\partial \phi / \partial x) = 0$ at $x = 0$, a.
This gives

$$B_{1n} = 0$$

and

$$B_{3n} = 0 \quad .$$

From Condition 2, $E_z = (\partial \phi / \partial z) = 0$ at $z = 0$, b. This gives

$$D_{1n} = 0$$

and

$$D_{3n} = 0 \quad .$$

Therefore, Eqs. 3.2 simplify to

$$\phi_1 = \sum_{n=0}^{\infty} A_n \cos \frac{n\pi}{a} x \cosh \gamma_n'(b - z) e^{-jKy} \qquad (3.3)$$

and

$$\phi_3 = \sum_{n=0}^{\infty} D_n \cos \frac{n\pi}{a} x \cosh \gamma_n' z e^{-jKy} , \qquad (3.4)$$

where A_n and D_n are unknown constants which will be determined when the potential functions and normal magnetic fields are matched at the slab interfaces.

3.3 Potential Fields in the YIG Region

The direction of the bias magnetic field in the cross-section plane can be chosen to be either parallel or normal to the YIG slab. In each case the partial differential equation for the potential fields in the YIG given by $\nabla \cdot (\bar{\bar{\mu}} \nabla \phi) = 0$ is dependent on the direction of magnetization. Therefore each case is analyzed separately.

1. Parallel magnetization. The relative permeability tensor when $\bar{H}_{dc}$ is in the x-direction (see Fig. 3.2) from Eq. 2.4b is written again as

$$\bar{\bar{\mu}}_r = \begin{bmatrix} 1 & 0 & 0 \\ 0 & \mu & jK_1 \\ 0 & -jK_1 & \mu \end{bmatrix} , \qquad (3.5)$$

where

$$\mu = 1 + \ldots$$

and

$$K_1 = \ldots$$

From Section 2.4.1, the potential function must satisfy the following equation:

FIG. 3.2 PARTIALLY LOADED WAVEGUIDE WITH $\bar{H}_{dc}$ PARALLEL TO THE

YIG SLAB.

$$\phi_{xx} + \mu\phi_{zz} = \mu K^2 \phi \ . \tag{3.6}$$

The following form is a solution to eq. 3.6 and satisfies boundary condition 1 (Section 2.4.2) in the YIG region (II):

$$\phi_2 = \sum_{n=0}^{\infty} \cos \frac{n\pi}{a} x (B_n \cosh \gamma_n z + C_n \sinh \gamma_n z) e^{-jKy} \ , \tag{3.7}$$

where B_n and C_n are arbitrary constants and

$$\gamma_n = \left[K^2 + \frac{1}{\mu}\left(\frac{n\pi}{a}\right)^2 \right]^{\frac{1}{2}} \ . \tag{3.8}$$

2. Normal magnetization. The dc magnetic field is in the z-direction (see Fig. 3.3) and the relative permeability tensor from Eq. 2.4a is given by

$$\mu_2 = \begin{pmatrix} \mu & jK_1 & 0 \\ -jK_1 & \mu & 0 \\ 0 & 0 & 1 \end{pmatrix} \ . \tag{3.9}$$

From eqs. 2.3a, 3.9 satisfies the following equation:

$$\phi_{xx} + \phi \ldots = \ldots \tag{3.10}$$

A potential function is assumed to have the following general form:

$$\phi = \sum_{n=} (B_n \cosh \gamma_n' z + C_n \sinh \gamma_n' z)(\ldots + D_n \sin q_n x) e^{-jKy} \tag{3.11}$$

where B_n, C_n ..... and D_n are .... while ....

$$\gamma_n' = \ldots + \ldots$$

FIG. 3.3 PARTIALLY LOADED WAVEGUIDE WITH $\overline{H}_{dc}$ NORMAL TO THE YIG SLAB.

Applying boundary condition 1 (Section 2.4.2), i.e., $b_x =$
$\mu(\partial\phi/\partial x) + K_1 K\phi = 0$ at $x = 0, a$, gives

$$\mu E_n \alpha_n + K_1 K F_n = 0 \tag{3.12a}$$

and

$$(-\mu E_n \alpha_n + K_1 K F_n) \sin \alpha_n a + (\mu E_n \alpha_n + K_1 K F_n) \cos \alpha_n a = 0 . \tag{3.12b}$$

Equations 3.12 give the following solutions:

$$\alpha_n = \frac{n\pi}{a} \tag{3.13a}$$

and

$$F_n = -\frac{K_1 K}{\mu\left(\frac{n\pi}{a}\right)} E_n . \tag{3.13b}$$

Physically, when the bias field is perpendicular to the slab
plane, the mode of propagation is the forward volume wave as discussed
in Section 2.4.3. For this mode the range of propagation is limited
to the range[52] where $\mu < 0$. Considering that propagation can exist
only for the $\mu < 0$ range of frequency, the phase constant β_n' becomes
$j\bar{\beta}_n$ and therefore all the hyperbolic function expansions in the
x-direction turn into expansions of sine and cosine terms. With the
help of the above consideration and the values given by Eq. 3.12,
Eq. 3.11 can now be written as

$$\psi = \cdots \tag{3.14}$$

where

$$\cdots$$

Equation 3.14 represents the potential ... ...

slab in terms of the unknown constants ...

potential functions at the slab interfaces ...

relation and allows the determination ...

3.4 Dispersion Relation

To obtain the dispersion relation, ...

3 and 5 from Section 2.4.2 must be applied in ...

magnetization case as follows:

1. Parallel magnetization. Condition 3 requires the continuity

of the potential functions 3.3 and 3.4 (in air) and 3.7 (in YIG) at

$z = z_1, z_2$. This gives

$$\sum_{n=0}^{\infty} A_n \cos \frac{n\pi}{a} x \cosh \gamma_n'(b - z_2) e^{-jKy} = \sum_{n=0}^{\infty} \cos \frac{n\pi}{a} x(B_n \cosh \gamma_n z_2$$

$$+ C_n \sinh \gamma_n z_2) e^{-jKy} \quad (3.15a)$$

and

$$\sum_{n=0}^{\infty} D_n \cos \frac{n\pi}{a} x \cosh \gamma_n' z_1 e^{-jKy} = \sum_{n=0}^{\infty} \cos \frac{n\pi}{a} x(B_n \cosh \gamma_n z_1$$

$$+ C_n \sinh \gamma_n z_1) e^{-jKy} \quad . \quad (3.15b)$$

Condition 5 requires continuity of b_z at the interfaces

$z = z_1$ and z_2 which, upon equating (from Eqs. 3.3, 3.4 and 3.7), gives

$$\sum_{n=0}^{\infty} - A_n \gamma_n' \cos \frac{n\pi}{a} x \sinh \gamma_n'(b - z_2) = \sum_{n=0}^{\infty} \cos \frac{n\pi}{a} x[B_n(- K_1 K \cosh \gamma_n z_2$$

$$+ \mu \gamma_n \cosh \gamma_n z_2) + C_n(- K_1 K \sinh \gamma_n z_2 + \mu \gamma_n \cosh \gamma_n z_2)] \quad (3.15c)$$

and

$$\sum_{n=0}^{\infty} D_n \gamma_n' \cos \frac{n\pi}{a} x \sinh \gamma_n' z_1 = \sum_{n=0}^{\infty} \cos \frac{n\pi}{a} x \{B_n(- K_1 K \cosh \gamma_n z_1$$

$$+ \mu \gamma_n \sinh \gamma_n z_1) + C_n(- K_1 K \sinh \gamma_n z_1 + \mu \gamma_n \cosh \gamma_n z_1)\} \quad . \quad (3.15d)$$

It follows from Eqs. 3.15 that each mode n is uncoupled to the others
and thus:

$$A_n \gamma_n' \sinh \gamma_n'(b - z_2) = - B_n(- K_1 K \cosh \gamma_n z_2 + \mu \gamma_n \sinh \gamma_n z_2)$$

$$- C_n(- K_1 K \sinh \gamma_n z_2 + \mu \gamma_n \cosh \gamma_n z_2) = 0 \quad ,$$

$$A_n \cosh \gamma_n'(b - z_2) = B_n \cosh \gamma_n z_2 + C_n \sinh \gamma_n z_2 \quad ,$$

$$D_n \cosh \gamma_n' z_1 = B_n \cosh \gamma_n z_1 + C_n \sinh \gamma_n z_1$$

and

$$D_n \gamma_n' \sinh \gamma_n' z_1 = B_n(- K_1 K \cosh \gamma_n z_1 + \mu \gamma_n \sinh \gamma_n z_1)$$

$$+ C_n(- K_1 K \sinh \gamma_n z_1 + \mu \gamma_n \cosh \gamma_n z_1) \quad .$$

When stated in matrix form, the following is obtained:

$$
\begin{bmatrix}
\gamma'_n \sinh \gamma'_n(b-z_2) & -K_1K \cosh \gamma_n z_2 + \mu\gamma_n \sinh \gamma_n z_2 & -K_1K \sinh \gamma_n z_2 + \mu\gamma_n \cosh \gamma_n z_2 & 0 \\
\cosh \gamma'_n(b-z_2) & -\cosh \gamma_n z_2 & -\sinh \gamma_n z_2 & 0 \\
0 & \cosh \gamma_n z_1 & \sinh \gamma_n z_1 & -\cosh \gamma'_n z_1 \\
0 & -K_1K \cosh \gamma_n z_1 + \mu\gamma_n \sinh \gamma_n z_1 & -K_1K \sinh \gamma_n z_1 + \mu\gamma_n \cosh \gamma_n z_1 & -\gamma'_n \sinh \gamma'_n z_1
\end{bmatrix}
\begin{bmatrix}
A_n \\
B_n \\
C_n \\
D_n
\end{bmatrix}
= 0
$$

$$. \tag{3.16}$$

The existence of nontrival solutions for A_n, B_n, C_n and D_n requires the determinant of the coefficient matrix in Eq. 3.16 to be zero. This yields the following dispersion relation:

$$- \tanh \gamma_n t [K_1^2 K^2 - \mu^2 \gamma_n^2 - \gamma_n'^2 \tanh \gamma_n' s_2 \tanh \gamma_n' s_1 - K_1 K \gamma_n (\tanh \gamma_n' s_2 - \tanh \gamma_n' s_1)] + \mu \gamma_n \gamma_n' (\tanh \gamma_n' s_2 + \tanh \gamma_n' s_1) = 0 \quad , \quad (3.17)$$

where t is the thickness of the YIG slab and s_1 and s_2 are the thicknesses of air regions III and I.

An alternate form of Eq. 3.17 is given by

$$e^{2\gamma_n t} = \frac{(\mu \gamma_n - K_1 K - \gamma_n' \tanh \gamma_n' s_1)(\mu \gamma_n + K_1 K - \gamma_n' \tanh \gamma_n' s_2)}{(\mu \gamma_n + K_1 K + \gamma_n' \tanh \gamma_n' s_1)(\mu \gamma_n - K_1 K + \gamma_n' \tanh \gamma_n' s_2)} \quad .$$

$$(3.18)$$

Equations 3.17 and 3.18 are exact dispersion equations which determine the frequency range of propagation of each mode independent of the existence of the other modes.

These equations reduce to simpler forms when some or all of the metallic boundary surfaces are driven to infinity. All these cases are studied under the heading of degenerate cases in a later section.

2. Normal magnetization. Matching the potential functions and normal magnetic fields in the air (Eqs. 3.3 and 3.4) and in YIG (Eq. 3.14) at the interfaces $x = x_1$ and x_2 on the basis of Conditions 3 and 5 given in Section 2.4.2 gives

$$\sum_{n=0}^{\infty} A_n \cosh \gamma_n'(b - z_2) \cos \frac{n\pi}{a} x\ e^{-jKy} = \sum_{n=0}^{\infty} \left(\cos \frac{n\pi}{a} x\right.$$

$$\left. - \frac{K_1 Ka}{\mu n\pi} \sin \frac{n\pi}{a} x\right)(B_n \cos \tilde{\gamma}_n z_2 + C_n \sin \tilde{\gamma}_n z_2)\ e^{-jKy} \quad , \quad (3.19a)$$

$$\sum_{n=0}^{\infty} - \gamma_n' A_n \sinh \gamma_n'(b - z_2) \cos \frac{n\pi}{a} x\ e^{-jKy} = \sum_{n=0}^{\infty} \tilde{\gamma}_n \left(\cos \frac{n\pi}{a} x\right.$$

$$\left. - \frac{K_1 Ka}{\mu n\pi} \sin \frac{n\pi}{a} x\right)(B_n \sin \tilde{\gamma}_n z_2 + C_n \cos \tilde{\gamma}_n z_2)\ e^{-jKy} \quad , \quad (3.19b)$$

$$\sum_{n=0}^{\infty} D_n \cosh \gamma_n' z_1 \cos \frac{n\pi}{a} x\ e^{-jKy} = \sum_{n=0}^{\infty} \left(\cos \frac{n\pi}{a} x - \frac{K_1 Ka}{\mu n\pi} \sin \frac{n\pi}{a} x\right)$$

$$\cdot (B_n \cos \tilde{\gamma}_n z_1 + C_n \sin \tilde{\gamma}_n z_1)\ e^{-jKy} \quad (3.19c)$$

and

$$\sum_{n=0}^{\infty} D_n \gamma_n' \sinh \gamma_n' z_1 \cos \frac{n\pi}{a} x\ e^{-jKy} = \sum_{n=0}^{\infty} \tilde{\gamma}_n \left(\cos \frac{n\pi}{a} x\right.$$

$$\left. - \frac{K_1 Ka}{\mu n\pi} \sin \frac{n\pi}{a} x\right)(B_n \sin \tilde{\gamma}_n z_1 + C_n \cos \tilde{\gamma}_n z_1)\ e^{-jKy} \quad . \quad (3.19d)$$

As can be seen in Eqs. 3.19, all modes except the zeroth order are coupled and one cannot exist without the others. This phenomenon leads to mode coupling which complicates the elimination of the unknown constants, A_n, B_n, C_n and D_n, in order to find the dispersion relation. However, the following procedure is adopted to obtain the dispersion relation: Multiplying both sides of Eqs. 3.19 by $\cos (m\pi/a)x$, integrating along the interface from 0 to a and noting that

$$\int_0^a \cos \frac{m\pi}{a} x \sin \frac{n\pi}{a} x \, dx = \begin{cases} 0 & n = m \\ 0 & n \neq m \quad, \quad n \pm m = \text{even} \\ \dfrac{2na}{\pi(n^2 - m^2)} & n \neq m \quad, \quad n \pm m = \text{odd} \end{cases}$$

yields the following results:

$$A_m \cosh \gamma_m'(b - z_2) - B_m \cos \tilde{\gamma}_m z_2 - C_m \sin \tilde{\gamma}_m z_2 + \frac{4K_1 Ka}{\mu\pi^2}$$

$$\sum_{\substack{n=0 \\ n\pm m=\text{odd}}}^{\infty} \frac{1}{n^2 - m^2} (B_n \cos \tilde{\gamma}_n z_2 + C_n \sin \tilde{\gamma}_n z_2) = 0 \quad, \quad (3.20a)$$

$$A_m \gamma_m' \sinh \gamma_m'(b - z_2) + \tilde{\gamma}_m (B_m \sin \tilde{\gamma}_m z_2 + C_m \cos \tilde{\gamma}_m z_2) - \frac{4K_1 Ka}{\mu\pi^2}$$

$$\sum_{\substack{n=0 \\ n\pm m=\text{odd}}}^{\infty} \frac{\tilde{\gamma}_n}{n^2 - m^2} (B_n \sin \tilde{\gamma}_n z_2 + C_n \cos \tilde{\gamma}_n z_2) = 0 \quad, \quad (3.20b)$$

$$D_m \cosh \gamma_m' z_1 - B_m \cos \tilde{\gamma}_m z_1 - C_m \sin \tilde{\gamma}_m z_1 + \frac{4K_1 Ka}{\mu\pi^2}$$

$$\sum_{\substack{n=0 \\ n\pm m=\text{odd}}}^{\infty} \frac{1}{n^2 - m^2} (B_n \cos \tilde{\gamma}_n z_1 + C_n \sin \tilde{\gamma}_n z_1) = 0 \quad (3.20c)$$

and

$$D_m \gamma_m' \sinh \gamma_m' z_1 - \tilde{\gamma}_m (B_m \sin \tilde{\gamma}_m z_1 + C_m \cos \tilde{\gamma}_m z_1) + \frac{4K_1 Ka}{\mu\pi^2}$$

$$\sum_{\substack{n=0 \\ n\pm m=\text{odd}}}^{\infty} \frac{\gamma_n}{n^2 - m^2} (B_n \sin \tilde{\gamma}_n z_1 + C_n \cos \tilde{\gamma}_n z_1) = 0 \quad. \quad (3.20d)$$

Upon elimination of A_n and D_n from Eqs. 3.20 the following system of linear equations is obtained:

$$B_m R_{mm} + C_m S_{mm} + P \sum_{\substack{n=o \\ n\pm m=odd}}^{\infty} (B_n R_{mn} + C_n S_{mn}) = 0 \qquad (3.21a)$$

and

$$B_m R'_{mm} + C_m S'_{mm} + P \sum_{\substack{n=o \\ n\pm m=odd}}^{\infty} (B_n R'_{mn} + C_n S'_{mn}) = 0 \ , \qquad (3.21b)$$

where

$$R_{mn} = \beta_{mn}(\gamma'_m \tanh \gamma'_m s_2 \cos \tilde{\gamma}_n z_2 - \tilde{\gamma}_n \sin \tilde{\gamma}_n z_2) \ ,$$

$$S_{mn} = \beta_{mn}(\gamma'_m \tanh \gamma'_m s_2 \sin \tilde{\gamma}_n z_2 + \tilde{\gamma}_n \cos \tilde{\gamma}_n z_2) \ ,$$

$$R'_{mn} = \beta_{mn}(\gamma'_m \tanh \gamma'_m z_1 \cos \tilde{\gamma}_n z_1 + \tilde{\gamma}_n \sin \tilde{\gamma}_n z_1) \ ,$$

$$S'_{mn} = \beta_{mn}(\gamma'_m \tanh \gamma'_m z_1 \sin \tilde{\gamma}_n z_1 - \tilde{\gamma}_n \cos \tilde{\gamma}_n z_1) \ ,$$

$$\beta_{mn} = \begin{cases} 1 & m = n \\ \dfrac{1}{n^2 - m^2} & m \neq n \end{cases} \ ,$$

$$s_2 = b - z_2$$

and

$$P = - 4K_1 Ka/\mu\pi^2 \ .$$

Equations 3.21 provide an infinite number of linear equations in B_n and C_n which can be expressed in the following form:

$$
\begin{bmatrix}
M_{11} & PM_{12} & \cdot & PM_{1i} & \cdot \\
PM_{21} & M_{22} & \cdot & PM_{2i} & \cdot \\
\cdot & \cdot & \cdot & \cdot & \cdot \\
\cdot & \cdot & \cdot & \cdot & \cdot \\
PM_{i1} & PM_{i2} & \cdot & M_{ii} & \cdot \\
\cdot & \cdot & \cdot & \cdot & \cdot
\end{bmatrix}
\begin{bmatrix}
N_1 \\
N_2 \\
\cdot \\
\cdot \\
N_i \\
\cdot
\end{bmatrix}
= 0 \quad , \qquad (3.22)
$$

where

$$
M_{ij} = \begin{bmatrix} R_{ij} & S_{ij} \\ R'_{ij} & S'_{ij} \end{bmatrix} \quad \begin{array}{l} \text{for } i \pm j = \text{odd} \\ \text{and } i = j \end{array} \quad ,
$$

$$
M_{ij} = 0 \quad i \pm j = \text{even}
$$

and

$$
N_i = \begin{bmatrix} B_i \\ C_i \end{bmatrix} \quad .
$$

A nontrivial and unique solution of Eq. 3.22 for N_i's exists if the infinite determinant of the coefficient matrix is set to zero. In numerical computation, the infinite determinant is truncated to a finite order. The accuracy of the truncation and numerical results are discussed in Chapter V.

3.5 Degenerate Cases

It is interesting to note that several degenerate cases of the formulation derived earlier reduce to problems that have been investigated previously.[37-42,61-66] These are:

1. The case of parallel magnetization. Three different structures are studied in this case.

a. Filled guide. This case corresponds to $s_1 = 0$ and $s_2 = 0$ and was presented in Case 4 of Section 2.4.4. From Eq. 3.17 the following is obtained:

$$(\tanh \gamma_n b)(K_1^2 K^2 + \mu^2 \gamma_n^2) = 0 \; . \tag{3.23}$$

Setting the term in the first parentheses to zero in Eq. 3.23 gives

$$\tanh (\gamma_n b) = 0 \; . \tag{3.24}$$

If $\mu < 0$, the solution to Eq. 3.24 is given by

$$\gamma_n = j \frac{n\pi}{b} \; . \tag{3.25}$$

Combining Eq. 3.25 with Eq. 3.8 yields Eq. 2.24 precisely.

Setting the terms in the second parentheses to zero gives

$$\gamma_n^2 = - K_1^2 K^2 / \mu \; . \tag{3.26}$$

Combining Eq. 3.26 with Eq. 3.8 yields Eq. 2.25.

b. Infinite-width YIG between ground planes. If $a \to \infty$, the problem reduces to that of Case 2 in Section 2.4.4. Equation 3.17 yields the same equation as Eq. 2.20 upon proper substitution.

c. Infinite-width slab in free space. Letting $a \to \infty$, $s_1 \to \infty$, $s_2 \to \infty$ reduces the problem to that of Case 1 in Section 2.4.4 and Eq. 3.17 in this case corresponds to Eq. 2.17.

2. Normal magnetization. Here one simple case of interest is derived and the other cases simply follow the same procedure. Through analysis, it was found that the zeroth-order mode is uncoupled and corresponds to the case when $a \to \infty$, i.e., when the YIG slab is

placed between two ground planes. This structure as shown in Fig. 3.4 has been investigated extensively.[37,40]

To derive the dispersion relation, the determinant of the zeroth-order matrix (M_{oo}) from Eq. 3.22 must be set to zero as follows:

$$\det (M_{oo}) = 0 \rightarrow \begin{vmatrix} R_{oo} & S_{oo} \\ R'_{oo} & S'_{oo} \end{vmatrix} = 0$$

and

$$R_{oo}S'_{oo} - R'_{oo}S_{oo} = 0 \quad . \tag{3.27}$$

Upon substitution and simplification, Eq. 3.27 becomes

$$\tan (\alpha K t) = \frac{\alpha(\tanh K s_2 + \tanh K z_1)}{\alpha^2 - \tanh K s_2 \tanh K z_1} \quad , \tag{3.28}$$

where

$$\alpha^2 = -\varepsilon \quad , \quad \varepsilon > 0 \quad .$$

Equation 3.28 is given by Ishii et al.[43]

FIG. 3.4 YIG SLAB BETWEEN TWO GROUND PLANES (NORMAL FIELD).

4.1 Introduction

The problem of magnetostatic-wave propagation in a ferrite slab of finite width inside a waveguide is analyzed. The analysis developed in this chapter is based on the integral equation method as follows:

1. An unknown potential function inside the ferrite slab is assumed. For clarity, the potential function for all the points inside the slab is denoted by $\tilde{\phi}_1(x,y,z)$.

2. Based on $\tilde{\phi}_1(x,y,z)$, fictitious "magnetic sources" (ρ_{m_1}) can be obtained as follows:

$$\overline{h}_1 = \nabla\tilde{\phi}_1 ,$$

$$\overline{b}_1 = \mu_0 \overline{\mu}_r \overline{h}_1 ,$$

$$\overline{m}_1 = \frac{\overline{b}_1}{\mu_0} - \overline{h}_1 ,$$

and the total magnetic charge (ρ_{m_1}) is

$$\rho_{m_1} = \rho_{v_1} + \rho_{s_1} ,$$

where

$$\rho_{v_1} = -\nabla \cdot \overline{m}_1 \quad \text{volume charges} ,$$

$$\rho_{s_1} = \overline{m}_1 \cdot \hat{n} \quad \text{surface charges}$$

and $\hat{n}$ is a unit vector normal to the surface. The magnetic charges, as described previously, are given in terms of $\tilde{\phi}_1(x,y,z)$.

3. By means of the "magnetic sources" and appropriate Green's function an integral expression for the potential function everywhere inside the waveguide (including the ferrite) can be written as follows:

$$\phi_1(x,y,z) = \iiint\limits_{\substack{YIG \\ volume}} \rho_v(x',y',z')G_1(x,y,z)\,dv'$$

$$+ \iint\limits_{\substack{YIG \\ surfaces}} \rho_s(x',y',z')G_1(x,y,z)\,ds' \quad , \quad (4.1)$$

where $\phi_1(x,y,z)$ is the potential function, G_1 is the Green's function, (x,y,z) is the observation point and (x',y',z') is the source point.

4. Assuming wave propagation in the y-direction, the y-variation of all functions involved in this study is therefore of the form e^{-jKy}. In this manner the following can be written:

$$\phi_1(x,y,z) = \phi(x,z)\,e^{-jKy} \quad ,$$

$$\tilde{\phi}_1(x,y,z) = \tilde{\phi}(x,z)\,e^{-jKy} \quad ,$$

$$G_1(x,y,z) = G(x,z)\,e^{-jKy} \quad ,$$

$$b_1(x,y,z) = b(x,z)\,e^{-jKy} \quad ,$$

$$h_1(x,y,z) = h(x,z)\,e^{-jKy} \quad ,$$

$$m_1(x,y,z) = m(x,z)\,e^{-jKy} \quad ,$$

$$\rho_{v_1}(x,y,z) = \rho_v(x,z)\,e^{-jKy}$$

and

$$\rho_{s_1}(x,y,z) = \rho_s(x,z)\,e^{-jKy} \quad .$$

In all the subsequent expressions, the factor $e^{-i\omega t}$ is omitted for simplicity.

The derivation of the mode of interaction and wave propagation in the small length would simplify Eq. 4.1 greatly as follows:

$$\phi(x,z) = \iint_{\substack{\text{YIG} \\ \text{area}}} \rho_v(x',z')G(x,z)\,dx'\,dz' + \int_{\substack{\text{YIG} \\ \text{fiber}}} \rho_s(x',z')G(x,z)\,d\ell' \;,$$

$$(4.2)$$

where $d\ell'$ is either dx' or dz' depending on where the charges are located.

b. The integral expression in Eq. 4.2 is two dimensional and very difficult to analyze. Assuming the slab to be very thin makes this equation one dimensional and tractable.

c. If only the points located inside the ferrite slab are considered, then from Eq. 4.2 an integral or more precisely an integro-differential equation in terms of ϕ is obtained. Solving the equation so obtained would lead to a very large determinant for the dispersion relation. For numerical analysis of this determinant, it must be properly truncated. Details of the truncated determinant along with the numerical results are discussed in Chapter 5.

4. Green's Function

The Green's function $G(x,z)$ must satisfy the following differential equation:

$$\left[\frac{\partial^2}{\partial x^2} + \frac{\partial^2}{\partial z^2}\right]G(x,z) = G''(x,z) = \delta(x - x')\,\delta(z - z') \quad . \quad (4.3)$$

This is the problem of finding the potential created by line charge extending along the y-axis with a location $x = x'$ and $z = z'$ and

Fig. 4.1). The boundary condition on $G(x,z)$ is that its normal derivatives should vanish on the four sidewalls.

Following the conventional approach,[67] $G(x,z)$ can be expressed as follows:

$$G(x,z) = G_1(x,z)U(z' - z) + G_2(x,z)U(z - z') , \qquad (4.4)$$

where $G_1(x,z)$ and $G_2(x,z)$ satisfy the homogeneous partial differential equation:

$$\left(\frac{\partial^2}{\partial x^2} + \frac{\partial^2}{\partial z^2}\right)G(x,z) - K^2 G(x,z) = 0 . \qquad (4.5)$$

The boundary conditions for G_1 and G_2 are:

$$\frac{\partial G_{1,2}}{\partial x} = 0 \text{ at } x = 0 , x = a ,$$

$$\frac{\partial G_1}{\partial z} = 0 \text{ at } z = 0$$

and

$$\frac{\partial G_2}{\partial z} = 0 \text{ at } z = b .$$

Formal solutions for $G_1(x,z)$ and $G_2(x,z)$ can now be written as

$$G_1(x,z) = \sum_{n=0}^{\infty} A_n \cos\frac{n\pi}{a} x \cosh \gamma_n' z \quad z < z' \qquad (4.6a)$$

and

$$G_2(x,z) = \sum_{n=0}^{\infty} B_n \cos\frac{n\pi}{a} x \cosh \gamma_n'(b - z) \quad z > z' , \qquad (4.6b)$$

where A_n, B_n are some unknown constants and $\gamma_n' = [K^2 + (n\pi/a)^2]^{1/2}$. To determine A_n and B_n, the boundary conditions at $z = z'$ (source) are applied as follows:

1. The continuity of G at $x = x'$ and $z = z'$ gives

FIG. 4.1 LINE SOURCE INSIDE A WAVEGUIDE.

$$A_n \cosh \gamma_n' z' = B_n \cosh \gamma_n'(b - z') \quad . \tag{4.7}$$

2. To obtain the second source condition, Eq. 4.3 is integrated from $z' - \epsilon$ to $z' + \epsilon$ where ϵ is a very small number. This gives

$$\left.\frac{\partial G_{2z}}{\partial z}\right|_{z'} - \left.\frac{\partial G_{1z}}{\partial z}\right|_{z'} = \frac{2}{a(1 + \delta_{on})} \cos \frac{n\pi}{a} x' \quad . \tag{4.8}$$

Differentiation of Eq. 4.6 and substitution in Eq. 4.8 gives

$$B_n \sinh \gamma_n'(b - z') - A_n \sinh \gamma_n' z' = \frac{2}{\gamma_n' a(1 + \delta_{on})} \cos \frac{n\pi}{a} x' \quad . \tag{4.9}$$

From Eqs. 4.7 and 4.9, A_n and B_n are obtained:

$$A_n = -\frac{2}{\gamma_n' a(1 + \delta_{on})} \frac{\cos \frac{n\pi}{a} x' \cosh \gamma_n'(b - z')}{\sinh \gamma_n' b} \tag{4.10a}$$

and

$$B_n = -\frac{2}{\gamma_n' a(1 + \delta_{on})} \frac{\cos \frac{n\pi}{a} x' \cosh \gamma_n' z'}{\sinh \gamma_n' b} \quad . \tag{4.10b}$$

Using Eqs. 4.6 and 4.10 yields the Green's function $G(x,z)$ from Eq. 4.4 in the final form:

$$G(x,x',z,z') = \sum_{n=0}^{\infty} \left(-\frac{2}{\gamma_n' a(1 + \delta_{on}) \sinh \gamma_n' b} \right) \cos \frac{n\pi}{a} x' \cos \frac{n\pi}{a} x$$

$$\cdot \cosh \gamma_n'(b - z') \cosh \gamma_n' z \, U(z' - z) + \sum_{n=0}^{\infty} \left(-\frac{2}{\gamma_n' a(1 + \delta_{on}) \sinh \gamma_n' b} \right)$$

$$\cdot \cos \frac{n\pi}{a} x' \cos \frac{n\pi}{a} x \cosh \gamma_n' z' \cosh \gamma_n'(b - z) U(z - z') \quad . \tag{4.11}$$

4.3 Equivalent Sources

In order to be able to solve the integral equation in terms of the potential inside the YIG slab, the magnetic charges must be determined. Mathematically, the source of magnetic charges can be considered to be the YIG slab. The mathematical form of the magnetic charges in terms of $\tilde{\phi}$ strongly depends on the permeability tensor which itself is a function of magnetic bias field direction. In this work parallel and normal magnetization are studied and therefore the magnetic charges are derived separately for each case.

To derive the magnetic charges, the small-signal magnetization vector $(\overline{m})$ must be determined. When the magnetostatic approximation discussed in Section 2.4.1 is used, the magnetic field intensity $(\overline{h})$ in the slab can be derived as the gradient of a scalar potential function $\tilde{\phi}(x,z)$. Finding $\overline{h}$ in terms of $\tilde{\phi}(x,z)$ leads to determination of $\overline{m}$ and eventually to ρ_m as follows:

$$\rho_m = \rho_v + \rho_s , \tag{4.12}$$

where

$$\rho_v = - \nabla \cdot \overline{m} + jkm_y , \tag{4.13a}$$

$$\rho_s = \overline{m} \cdot \hat{n} \tag{4.13b}$$

and $\hat{n}$ is a unit vector normal to the slab surface. The small-signal magnetization $(\overline{m})$ is given by

$$\overline{m} = \frac{\overline{b}}{\mu_0} - \overline{h} , \tag{4.14}$$

where

$$\overline{h} = \nabla \phi - jk\phi\hat{y} , \tag{4.15}$$

$$\overline{b} = \mu_0 \overline{\overline{\mu}} \cdot \overline{h}$$

and $\overline{\overline{\mu}}_r$ is the permeability tensor derived in Section 2.2. Substitution for $\overline{b}$ and $\overline{h}$ in Eq. 4.14 gives

$$\overline{m} = (\overline{\overline{\mu}}_r - \overline{\overline{I}}) \cdot (\nabla \tilde{\phi} - jK\tilde{\phi}\hat{y}) \quad , \qquad (4.16)$$

where $\overline{\overline{I}}$ is the identity tensor, i.e., all elements are zero except the diagonal elements which are 1.

Thus with the help of Eq. 4.16, surface and volume charges from Eqs. 4.13 can be written as:

$$\rho_v = -\nabla \cdot [(\overline{\overline{\mu}}_r - \overline{\overline{I}}) \cdot (\nabla \tilde{\phi} - jK\tilde{\phi}\hat{y})] + jKm_y \qquad (4.17a)$$

and

$$\rho_s = [(\overline{\overline{\mu}}_r - \overline{\overline{I}}) \cdot (\nabla \tilde{\phi} - jK\tilde{\phi}\hat{y})] \cdot \hat{n} \quad . \qquad (4.17b)$$

From Eqs. 4.17 it can be seen clearly that the magnetic volume and surface charges depend upon the relative permeability tensor $(\overline{\overline{\mu}}_r)$. In the following sections, ρ_v and ρ_s are derived explicitly in terms of the scalar potential in the slab $(\tilde{\phi})$ for the two cases of parallel and normal magnetization.

4.3.1 Parallel Magnetization Charges. The relative permeability tensor from Section 2.2 for $\overline{H}_{dc}$ in the x-direction is given by (see Fig. 4.2):

$$\overline{\overline{\mu}}_r = \begin{pmatrix} 1 & 0 & 0 \\ 0 & \mu & jK_1 \\ 0 & -jK_1 & \mu \end{pmatrix} \quad . \qquad (4.18)$$

Substitutions from Eq. 4.18 into Eqs. 4.17 yields ρ_v and ρ_s as follows:

. . . . PARALLEL TO THE YIG SLAB.

$$\rho_V(x,z) = -\nabla \cdot \left\{ \left[-jK(\mu-1)\tilde{\phi} + jK_1 \frac{\partial\tilde{\phi}}{\partial z} \right]\hat{y} + \left[-K_1 K\tilde{\phi} + (\mu-1)\frac{\partial\tilde{\phi}}{\partial z} \right]\hat{z} \right\}$$

$$+ K^2(\mu-1)\tilde{\phi} - K_1 K \frac{\partial\tilde{\phi}}{\partial z}$$

and

$$\rho_S(x,z) = \mp \left\{ \left[-jK(\mu-1)\tilde{\phi} + jK_1 \frac{\partial\tilde{\phi}}{\partial x} \right]\hat{y} + \left[-K_1 K\tilde{\phi} + (\mu-1)\frac{\partial\tilde{\phi}}{\partial z} \right]\hat{z} \right\}\cdot\hat{z} \quad ,$$

where the upper sign in ρ_S is for $z = z_1$ and the lower sign is for $z = z_2$. Carrying out the mathematical operations in these equations for ρ_V and ρ_S gives

$$\rho_V(x,z) = K^2(\mu-1)\tilde{\phi}(x,z) - (\mu-1)\frac{\partial^2\tilde{\phi}(x,z)}{\partial z^2} \tag{4.19}$$

and

$$\rho_S(x,z) = \begin{cases} \rho_{S_1} = K_1 K\tilde{\phi}(x,z_1) - (\mu-1)\dfrac{\partial\tilde{\phi}(x,z_1)}{\partial z} & \text{at } z = z_1 \\[2mm] \rho_{S_2} = -K_1 K\tilde{\phi}(x,z_2) + (\mu-1)\dfrac{\partial\tilde{\phi}(x,z_2)}{\partial z} & \text{at } z = z_2 \end{cases}$$

$$\tag{4.20}$$

It is to be noted that there are no surface charges at surfaces $x = x_0$ or $x = a - x_0$.

4.3.2 Normal Magnetization Charges. The relative permeability tensor from Section 2.2 is given by (see Fig. 4.3):

$$\bar{\bar{\mu}}_r = \begin{pmatrix} \mu & jK_1 & 0 \\ -jK_1 & \mu & 0 \\ 0 & 0 & 1 \end{pmatrix} . \tag{4.21}$$

If $\bar{\bar{\mu}}_r$ from above is used, Eqs. 4.17 for ρ_V and ρ_S can be written as:

FIG. 4.3 DEVICE CONFIGURATION FOR $\overline{H}_{dc}$ NORMAL TO THE YIG SLAB.

$$\rho_V = -\nabla \cdot \left\{ \left[(\mu - 1)\frac{\partial \tilde{\phi}}{\partial x} + K_1 K\tilde{\phi} \right] \hat{x} + \left[-jK_1 \frac{\partial \tilde{\phi}}{\partial x} - jK(\mu - 1)\tilde{\phi} \right] \hat{y} \right\}$$

$$+ K_1 K \frac{\partial \tilde{\phi}}{\partial x} - K^2(\mu - 1)\tilde{\phi} \quad (4.22a)$$

and

$$\rho_S = \mp \left\{ \left[(\mu - 1)\frac{\partial \tilde{\phi}}{\partial x} + K_1 K\tilde{\phi} \right] \hat{x} + \left[-jK_1 \frac{\partial \tilde{\phi}}{\partial x} - jK(\mu - 1)\tilde{\phi} \right] \hat{y} \right\} \cdot \hat{x} \quad (4.22b)$$

where the upper and lower signs are for charges at $x = x_o$, $a - x_o$, respectively. Upon performing the mathematical operations in the above and noting that (from Section 2.4.1):

$$\frac{\partial^2 \tilde{\phi}}{\partial z^2} + \mu\left(\frac{\partial^2 \tilde{\phi}}{\partial x^2} - K^2\tilde{\phi}\right) = 0 \quad ,$$

ρ_V and ρ_S are finally given by

$$\rho_V(x,z) = \frac{\mu - 1}{\mu} \frac{\partial^2 \tilde{\phi}}{\partial z^2}(x,z) \quad (4.23)$$

and

$$\rho_S(x,z) = \begin{cases} \rho_{S_1} = -(\mu - 1)\dfrac{\partial\tilde{\phi}(x_o,z)}{\partial x} - K_1 K\tilde{\phi}(x_o,z) \quad \text{at } x = x_o \\[3mm] \rho_{S_2} = (\mu - 1)\dfrac{\partial\tilde{\phi}(a - x_o,z)}{\partial x} + K_1 K\tilde{\phi}(a - x_o,z) \\[3mm] \qquad\qquad\qquad\qquad\qquad\qquad \text{at } x = a - x_o \quad . \quad (4.24) \end{cases}$$

From Eq. 4.24 it can be seen that the surface charges at $z = $: or z_2 are absent and the only existing surface charges are at $x = x_o$ and $x = a - x_o$. It will be seen that this difference in the charge arrangement and mathematical form for the two cases will lead to different formulations in each case.

4.4 Integral Equation

As discussed in Section 4.1, the integral equation (Eq. 4.2) can be obtained in terms of $\tilde{\phi}(x,z)$ if only the points inside the ferrite slab are considered. Since ρ_v and ρ_s are different for the two cases of parallel and normal magnetization, each case is considered separately.

4.4.1 Parallel Magnetization Formulation.

When the appropriate expression for ρ_v and ρ_s from Eqs. 4.19 and 4.20 is used and when points (x,z) are considered such that $\{(x,z), x_0 \lesseqgtr x \lesseqgtr a - x_0, z_1 \lesseqgtr z \lesseqgtr z_2\}$, Eq. 4.2 can be written as:

$$\tilde{\phi}(x,z) = \int_{x_0}^{a-x_0} \int_{z_1}^{z_2} [K^2(\mu - 1)\tilde{\phi}(x',z') - (\mu - 1)\tilde{\phi}_{zz}(x',z')]$$

$$\cdot G(x,x',z,z') \, dx' \, dz' + \int_{x_0}^{a-x_0} [K_1 K\tilde{\phi}(x',z_1) - (\mu - 1)\tilde{\phi}_z(x',z_1)]$$

$$\cdot G_1(x,x',z,z_1) \, dx' + \int_{x_0}^{a-x_0} [-K_1 K\tilde{\phi}(x',z_2) + (\mu - 1)\tilde{\phi}_z(x',z_2)]$$

$$\cdot G_2(x,x',z,z_2) \, dx' \quad . \quad (4.25)$$

The integro-differential equation (Eq. 4.25) is two-dimensional in (x,z) and is difficult to analyze. Thus the ferrite slab is assumed to be very thin such that $\tilde{\phi}(x,z)$ may be assumed to vary linearly in z. In this approximation two functions of one variable may be used to approximate $\tilde{\phi}(x,z)$ in the following manner. If

$$f_1(x) \stackrel{\triangle}{=} \tilde{\phi}(x,z_1)$$

and

$$f_2(x) \stackrel{\triangle}{=} \tilde{\phi}(x,z_2) \quad ,$$

then by linear approximation the following is obtained:

$$\tilde{\phi}(x,z) \cong f_1(x) + \frac{f_2(x) - f_1(x)}{z_2 - z_1}(z - z_1) \quad z_1 \leqq z \leqq z_2$$

or

$$\tilde{\phi}(x,z) \cong \frac{f_2(x)(z - z_1) + f_1(x)(z_2 - z)}{z_2 - z_1} \tag{4.26}$$

which gives

$$\tilde{\phi}_z(x,z) \cong \frac{f_2(x) - f_1(x)}{z_2 - z_1} \tag{4.27}$$

and

$$\tilde{\phi}_{zz}(x,z) \cong 0 \quad . \tag{4.28}$$

Substitution of Eqs. 4.26 through 4.28 in the integral equation (Eq. 4.25) yields

$$\tilde{\phi}(x,z) = \int_{x_0}^{a-x_0} \int_{z_1}^{z_2} K^2(\mu - 1)\left(\frac{f_2(x')(z' - z_1) + f_1(x')(z_2 - z')}{z_2 - z_1}\right)$$

$$\cdot G(x,x',z,z') \, dz' \, dx' - \int_{x_0}^{a-x_0}\left[- K_1 K\left(\frac{f_2(x')(z' - z_1) + f_1(x')(z_2 - z')}{(z_2 - z_1)}\right)\right.$$

$$+ (\mu - 1)\left(\frac{f_2(x') - f_1(x')}{(z_2 - z_1)}\right)\right] G_1(x,x',z,z_1) \, dx'$$

$$+ \int_{x_0}^{a-x_0}\left[- K_1 K\left(\frac{f_2(x')(z' - z_1) + f_1(x')(z_2 - z')}{(z_2 - z_1)}\right)\right.$$

$$+ (\mu - 1)\left(\frac{f_2(x') - f_1(x')}{(z_2 - z_1)}\right)\right] G_2(x,x',z,z_2) \, dx' \quad . \tag{4.29}$$

Evaluating the integral equation given by Eq. 4.29 at $z = z_1$, z_2 and substituting for Green's functions G_1 and G_2 from Eq. 4.11 gives

$$f_1(x) = \sum_{n=0}^{\infty} - \frac{2v_n}{a(1 + \delta_{on})} \cos \frac{n\pi}{a} x \cosh \gamma_n'z_1 \{I_{v_1} + I_{s_1}\} \qquad (4.30a)$$

and

$$f_2(x) = \sum_{n=0}^{\infty} - \frac{2v_n}{a(1 + \delta_{on})} \cos \frac{n\pi}{a} x \cosh \gamma_n'(b - z_2)\{I_{v_2} + I_{s_2}\} \ ,$$
$$(4.30b)$$

where

$$v_n = \frac{1}{\gamma_n' \sinh \gamma_n'b} \ ,$$

$$I_{v_1} = (\mu - 1)K^2 \int_{x_0}^{a-x_0} \left[\frac{f_2(x')(z' - z_1) + f_1(x')(z_2 - z')}{z_2 - z_1} \right] \cos \frac{n\pi}{a} x'$$

$$\cdot \cosh \gamma_n'(b - z') \ dz' \ dx' \ ,$$

$$I_{s_1} = - \int_{x_0}^{a-x_0} \left[- K_1K f_1(x') + (\mu - 1)\left(\frac{f_2(x') - f_1(x')}{z_2 - z_1} \right) \right] \cos \frac{n\pi}{a} x'$$

$$\cdot \cosh \gamma_n'(b - z_1) \ dx' + \int_{x_0}^{a-x_0} \left[- K_1K f_2(x') + (\mu - 1)\left(\frac{f_2(x') - f_1(x')}{z_2 - z_1} \right) \right]$$

$$\cdot \cos \frac{n\pi}{a} x' \cosh \gamma_n'(b - z_2) \ dx' \ ,$$

$$I_{v_2} = (\mu - 1)K^2 \int_{x_0}^{a-x_0} \int_{z_1}^{z_2} \left(\frac{f_2(x')(z' - z_1) + f_1(x')(z_2 - z')}{z_2 - z_1} \right)$$

$$\cdot \cos \frac{n\pi}{a} x' \cosh \gamma_n'z' \ dz' \ dx'$$

and

$$I_{S_2} = -\int_{x_o}^{a-x_o} \left[-K_1 K f_1(x) + (\mu - 1)\left(\frac{f_2(x') - f_1(x')}{z_2 - z_1}\right) \right] \cos \frac{n\pi}{a} x'$$

$$\cdot \cosh \gamma_n' z_1 \, dx' + \int_{x_o}^{a-x_o} \left[-K_1 K f_2(x) + (\mu - 1)\left(\frac{f_2(x') - f_1(x')}{z_2 - z_1}\right) \right]$$

$$\cdot \cos \frac{n\pi}{a} x' \cosh \gamma_n' z_2 \, dx' \quad .$$

Equations 4.30 are rewritten as follows when the integrations in the z-direction are carried out:

$$f_1(x) = -\sum_{n=o}^{\infty} \frac{2/a}{1 + \delta_{on}} \cos \frac{n\pi}{a} x(g_{11}^n C_1^n + g_{12}^n C_2^n) \qquad (4.31a)$$

and

$$f_2(x) = -\sum_{n=o}^{\infty} \frac{2/a}{1 + \delta_{on}} \cos \frac{n\pi}{a} x(g_{21}^n C_1^n + g_{22}^n C_2^n) \quad , \qquad (4.31b)$$

where

$$C_1^n = \int_{x_o}^{a-x_o} f_1(x) \cos \frac{n\pi}{a} x \, dx \quad ,$$

$$C_2^n = \int_{x_o}^{a-x_o} f_2(x) \cos \frac{n\pi}{a} x \, dx \quad ,$$

$$g_{11}^n = \frac{\cosh \gamma_n' z_1}{\gamma_n' \sinh \gamma_n' b} \left[(K_1 K - P_1) \cosh \gamma_n' s_1 + P_1 \cosh \gamma_n' s_2 \right.$$

$$\left. - P_2 \sinh \gamma_n' s_1 \right] \quad ,$$

$$g_{12}^n = \frac{\cosh \gamma_n' z_1}{\gamma_n' \sinh \gamma_n' b} \left[-(K_1 K + P_1) \cosh \gamma_n' s_2 + P_1 \cosh \gamma_n' s_1 \right.$$

$$\left. - P_2 \sinh \gamma_n' s_2 \right] \quad ,$$

$$\varepsilon_{21}^{n} = \frac{\cosh \gamma_n' s_2}{\gamma_n' \sinh \gamma_n' b} [(K_1 K - F_1) \cosh \gamma_n' z_1 + P_1 \cosh \gamma_n' z_2$$
$$- P_2 \sinh \gamma_n' z_1] \quad ,$$

$$\varepsilon_{22}^{n} = \frac{\cosh \gamma_n' s_2}{\gamma_n' \sinh \gamma_n' b} [-(K_1 K + F_1) \cosh \gamma_n' z_2 + P_1 \cosh \gamma_n' z_1$$
$$+ P_2 \sinh \gamma_n' z_2] \quad ,$$

$$F_1 = \frac{1 - \mu}{t} \left(\frac{n\pi}{a}\right)^2 \quad ,$$

$$P_2 = (\mu - 1) K^2 / \gamma_n' \quad ,$$

$$s_1 = b - z_1$$

and

$$s_2 = b - z_2 \quad .$$

Multiplication of Eqs. 4.31 by $\cos (m\pi/a)x$ and integration along the interface from $x = x_0$ to $x = (a - x_0)$ yields

$$C_1^m + \sum_{n=0}^{\infty} \alpha_{mn} [\varepsilon_{11}^n C_1^n + \varepsilon_{12}^n C_2^n] = 0 \tag{4.32a}$$

and

$$C_2^m + \sum_{n=0}^{\infty} \alpha_{mn} [\varepsilon_{21}^n C_1^n + \varepsilon_{22}^n C_2^n] = 0 \quad , \tag{4.32b}$$

where ($m \neq 0$, $n \neq 0$),

$$\alpha_{mn} = \begin{cases} 1 - \frac{2x_0}{a} - \frac{1}{n\pi} \sin \frac{n\pi x_0}{a} \quad , \quad m = n \\ -\frac{a}{\pi} \left(\frac{\sin (m - n)\pi x_0/a}{(m - n)} + \frac{\sin m + n\pi x_0/a}{(m + n)}\right) , \quad m + n = \text{even} \end{cases}$$

Equations 4.32 provide a system of linear equations in C_1^n and C_2^n which is infinite in number. Since even and ...

Eqs. 4.32 take the following form in matrix notation:

$$
\begin{bmatrix}
1 + M_{11} & M_{13} & \cdot & \cdot & \cdot & M_{1i} & \cdot & \cdot & \cdot \\
M_{31} & 1 + M_{33} & & & & \cdot & & & \\
\cdot & & \cdot & & & \cdot & & & \\
\cdot & & & \cdot & & \cdot & & & \\
\cdot & & & & \cdot & \cdot & & & \\
M_{i1} & \cdot & \cdot & \cdot & \cdot & 1 + M_{ii} & \cdot & \cdot & \cdot \\
& & & & & \cdot & & & \\
& & & & & \cdot & & & \\
& & & & & \cdot & & &
\end{bmatrix}
\begin{bmatrix}
C^1 \\ C^3 \\ \cdot \\ \cdot \\ \cdot \\ C^i \\ \cdot \\ \cdot \\ \cdot
\end{bmatrix}
= 0 \quad , \quad \text{odd modes only}
$$

$$(4.33a)$$

and

$$
\begin{bmatrix}
1 + M_{22} & M_{24} & \cdot & \cdot & \cdot & M_{2i} & \cdot & \cdot & \cdot \\
M_{42} & 1 + M_{44} & & & & \cdot & & & \\
\cdot & & \cdot & & & \cdot & & & \\
\cdot & & & \cdot & & \cdot & & & \\
\cdot & & & & \cdot & \cdot & & & \\
M_{i2} & \cdot & \cdot & \cdot & \cdot & 1 + M_{ii} & \cdot & \cdot & \cdot \\
& & & & & \cdot & & & \\
& & & & & \cdot & & & \\
& & & & & \cdot & & &
\end{bmatrix}
\begin{bmatrix}
C^2 \\ C^4 \\ \cdot \\ \cdot \\ \cdot \\ C^i \\ \cdot \\ \cdot \\ \cdot
\end{bmatrix}
= 0 \quad , \quad \text{even modes, only}
$$

$$(4.33b)$$

where M and C are matrices defined by:

$$
M_{ij} = \begin{bmatrix}
\alpha_{ij}\sigma^j_{11} & \alpha_{ij}\sigma^j_{12} \\
\alpha_{ij}\sigma^j_{21} & \alpha_{ij}\sigma^j_{22}
\end{bmatrix}
$$

and

$$
C^i = \begin{bmatrix} \cdot \\ \cdot \end{bmatrix} \cdot
$$

To obtain a nontrivial value solution to C^n's, the infinite
determinant of the coefficient matrix in Eqs. 4.33 must be zero.
In the numerical analysis, the infinite determinant is truncated
to order N. If the truncated determinant is defined as $D_N(f,K)$,
then the dispersion relation to be solved numerically for roots is
given by

$$D_N(f,K) = 0 . \qquad (4.34)$$

The discussion on the proper choice of N for reasonably accurate
results and the numerical data are presented in the next chapter.

   4.4.2 _Normal Magnetization Formulation_. The integral equation
for this case is developed by using the proper ρ_V and ρ_S given by
Eqs. 4.23 and 4.24. Thus, from Eq. 4.2 it follows that

$$\tilde{\phi}(x,z) = \int_{x_0}^{a-x_0} \int_{z_1}^{z_2} \left[\left(\frac{\mu-1}{\mu}\right) \tilde{\phi}_{zz}(x',z') \right] G(x,x',z,z') \, dz' \, dx'$$

$$- \int_{z_1}^{z_2} (\mu-1)\tilde{\phi}_x(x_0,z') + K_1 \tilde{K}\tilde{\phi}(x_0,z') G(x,x_0,z,z') \, dz'$$

$$+ \int_{z_1}^{z_2} (\mu-1)\tilde{\phi}_x(a-x_0,z') + K_1 \tilde{K}\tilde{\phi}(a-x_0,z') G(x,a-x_0,z,z') \, dz' .$$

$$(4.35)$$

Here again, the thin-disk approximation simplifies Eq. 4.35 into a
one-dimensional integral which is tractable.

   As noted in Eq. 4.2, the volume integral term involves a
second-order partial derivative term $\tilde{\phi}_{zz}$ which must be evaluated
properly. To evaluate $\tilde{\phi}_{zz}$, the volume is sub-
divided into two regions, namely, $z_1, \ldots, z_1 = z = z$

and $z_O \lesseqgtr z \lesseqgtr z_2$ (Fig. 4.3). The variation of $\tilde{\phi}(x,z)$ in each layer in the z-direction is assumed to be linear. In this manner three functions, each having one variable, are used to approximate $\tilde{\phi}(x,z)$ in the slab, as follows:

$$f_1(x) \triangleq \tilde{\phi}(x,z_1) \quad ,$$

$$f_O(x) \triangleq \tilde{\phi}(x,z_O)$$

and

$$f_2(x) \triangleq \tilde{\phi}(x,z_2) \quad .$$

The linear approximation gives

$$\tilde{\phi}(x,z) \cong \frac{f_1(x)(z_O - z) + f_O(x)(z - z_1)}{z_O - z_1} , z_1 \leqq z \leqq z_O \qquad (4.36a)$$

and

$$\tilde{\phi}(x,z) \cong \frac{f_O(x)(z_2 - z) + f_2(x)(z - z_O)}{z_2 - z_O} , z_O \leqq z \leqq z_2 \qquad (4.36b)$$

which gives

$$\tilde{\phi}_z(x,z) = \frac{f_O(x) - f_1(x)}{z_O - z_1} , z_1 \leqq z \leqq z_O \quad , \qquad (4.37a)$$

$$\tilde{\phi}_z(x,z) = \frac{f_2(x) - f_O(x)}{z_2 - z_O} , z_O \leqq z \leqq z_2 \qquad (4.37b)$$

and

$$\tilde{\phi}_{zz}(x,z) = \frac{f_2(x) - 2f_O(x) + f_1(x)}{d^2} , \qquad (4.38)$$

where $d = z_O - z_1 = z_2 - z_O = t/2$ and t is the slab thickness. In the integral equation (Eq. 4.29), the second and third terms are surface integrals over the sides of the slab at $x = x_O$ and $a - x_O$.

In the thin-slab assumption, instead of a continuous
distribution of surface charge in z, the charge distribution on both
sides of the slab (x_o and $a - x_o$) in each region $z_1 \lesseqgtr z \lesseqgtr z_o$ and
$z_o \lesseqgtr z \lesseqgtr z_2$ is assumed to be uniform. This uniform charge distribu-
tion assumption connotes that the surface charge in each region
is equal to the mean of its values at the edges of that region.

From Eqs. 4.24 the surface charge can be rewritten as

$$\rho_s(x_i,z) = \mp (\mu - 1)\tilde{\phi}_x(x_i,z) \mp K_1 K \tilde{\phi}(x_i,z) \quad , \qquad (4.39a)$$

where $x_i = x_o$ or $a - x_o$. Because of the uniform surface charge
distribution in the z-direction in each layer, it follows that

$$\phi(x_i,z) \cong \frac{f_1(x_i) + f_o(x_i)}{2} \quad z_1 \lesseqgtr z \lesseqgtr z_o$$

and

$$\phi(x_i,z) \cong \frac{f_2(x_i) + f_o(x_i)}{2} \quad z_o \lesseqgtr z \lesseqgtr z_2 \quad .$$

Therefore, Eq. 4.39a for $\rho_s(x_i,z)$ now becomes

$$\rho_s(x_i,z) \cong \begin{cases} \mp (\mu-1)\left(\dfrac{f'_1(x_i) + f'_o(x_i)}{2}\right) \mp K_1 K\left(\dfrac{f_1(x_i) + f_o(x_i)}{2}\right) & z_1 \lesseqgtr z \lesseqgtr z_o \\[4mm] \mp (\mu-1)\left(\dfrac{f'_2(x_i) + f'_o(x_i)}{2}\right) \mp K_1 K\left(\dfrac{f_2(x_i) + f_o(x_i)}{2}\right) & z_o \lesseqgtr z \lesseqgtr z_2 \end{cases}$$

$$. \qquad (4.39b)$$

The main reason for uniform charge distribution at the slab sides
($x = x_o$ and $a - x_o$) is the fact that $\phi(x,z)$ is evaluated only at
three values of z, i.e., $z = z_1$, z_o and z_2. The function ϕ between
these values is unknown and so all the equations should involve

calculations of $\tilde{\phi}(x,z)$ strictly at these three values of z. Thus continuous charge distribution would not be a plausible assumption under these conditions. Substituting from Eqs. 4.36 through Eqs. 4.39 into the integro-differential equation given by Eq. 4.35 yields

$$
\tilde{\phi}(x,z) = \int_{x_o}^{a-x_o} \int_{z_1}^{z_2} \left(\frac{\mu - 1}{\mu}\right) \left(\frac{f_2(x') - 2f_o(x') + f_1(x')}{d^2}\right)
$$

$$
\cdot\, G(x,x',z,z')\, dz'\, dx' - \int_{z_1}^{z_o} \left[(\mu - 1)\left(\frac{f_1'(x_o) + f_o'(x_o)}{2}\right) \right.
$$

$$
\left. + K_1 K\left(\frac{f_1(x_o) + f_o(x_o)}{2}\right) \right] G(x,x_o,z,z')\, dz' - \int_{z_o}^{z_2} \left[(\mu - 1) \right.
$$

$$
\cdot \left(\frac{f_2'(x_o) + f_o'(x_o)}{2}\right) + K_1 K\left(\frac{f_2(x_o) + f_o(x_o)}{2}\right) \right] G(x,x_o,z,z')\, dz'
$$

$$
+ \int_{z_1}^{z_o} \left[(\mu - 1)\left(\frac{f_1'(a - x_o) + f_o'(a - x_o)}{2}\right) + K_1 K\left(\frac{f_1(a - x_o) + f_o(a - x_o)}{2}\right) \right]
$$

$$
\cdot\, G(x,a - x_o, z, z')\, dz' + \int_{z_o}^{z_2} \left[(\mu - 1)\left(\frac{f_2'(a - x_o) + f_o'(a - x_o)}{2}\right) \right.
$$

$$
\left. + K_1 K\left(\frac{f_2(a - x_o) + f_o(a - x_o)}{2}\right) \right] G(x,a - x_o,z,z')\, dz' \quad . \tag{4.40}
$$

In Eq. 4.40, the z-integrals can be carried out easily and may be expressed in terms of one or more of the following constants:

$$
P_1^n = \int_{z_1}^{z_o} \cosh \gamma_n' z'\, dz' \quad ,
$$

$$B_2^n = \int_{z_0}^{z_2} \cosh \gamma_n' z' \, dz' \quad ,$$

$$B_3^n = \int_{z_1}^{z_0} \cosh \gamma_n'(b - z') \, dz'$$

and

$$B_4^n = \int_{z_0}^{z_2} \cosh \gamma_n'(b - z') \, dz' \quad .$$

Substituting for G from Eq. 4.11 and carrying out the z-integrals yields the following when Eq. 4.40 is evaluated at $z = z_1$, z_0 and z_2, respectively:

$$f_1(x) = - \sum_{n=0}^{\infty} \frac{2v_n}{a(1 + \delta_{on})} (B_3^n + B_4^n) \cosh \gamma_n' z_1 \cos \frac{n\pi}{a} x \int_{\lambda_0}^{a-x_0} \left(\frac{\mu - 1}{\mu} \right)$$

$$\cdot \frac{f_2(x') - 2f_0(x') + f_1(x')}{d^2} \cos \frac{n\pi}{a} x' \, dx' - \sum_{n=0}^{\infty} \frac{2v_n \cos \frac{n\pi}{a} x_0}{a(1 + \delta_{on})}$$

$$\cdot \cosh \gamma_n' z_1 \left[B_4^n \left(\frac{(\mu - 1)}{2} [f_2'(x_0) + f_0'(x_0)] + \frac{K_1 K}{2} [f_2(x_0) + f_0(x_0)] \right) \right.$$

$$\left. + B_3^n \left(\frac{(\mu - 1)}{2} [f_1'(x_0) + f_0'(x_0)] + \frac{K_1 K}{2} [f_1(x_0) + f_0(x_0)] \right) \right]$$

$$- \sum_{n=0}^{\infty} \frac{2v_n \cos \frac{n\pi}{a} (a - x_0)}{a(1 + \delta_{on})} \cosh \gamma_n' z_1 \left[B_4^n \left(\frac{(\mu - 1)}{2} [f_2'(a - x_0) \right. \right.$$

$$\left. + f_0'(a - x_0)] + \frac{K_1 K}{2} [f_2(a - x_0) + f_0(a - x_0)] \right) + B_3^n \left(\frac{(\mu - 1)}{2} [f_1'(a - x_0) \right.$$

$$\left. \left. + f_0'(a - x_0)] + \frac{K_1 K}{2} [f_1(a - x_0) + f_0(a - x_0)] \right) \right] \quad , \quad (4.41a)$$

$$f_o(x) = -\sum_{n=o}^{\infty} \frac{2v_n}{a(1 + \delta_{on})} \left[B_1^n \cosh \gamma_n'(b - z_o) + B_4^n \cosh \gamma_n' z_o \right]$$

$$\cdot \cos \frac{n\pi}{a} x \int_{x_o}^{a-x_o} \frac{\mu - 1}{\mu} \left(\frac{f_2(x') - 2f_o(x') + f_1(x')}{d^2} \cos \frac{n\pi}{a} x' \right) dx'$$

$$- \sum_{n=o}^{\infty} \frac{2v_n \cos \frac{n\pi}{a} x_o}{a(1 + \delta_{on})} \cos \frac{n\pi}{a} x \left[B_4^n \cosh \gamma_n' z_o \left(\frac{(\mu - 1)}{2} [f_2'(x_o) + f_o'(x_o)] \right. \right.$$

$$+ \frac{K_1 K}{2} [f_2(x_o) + f_o(x_o)] \right) + B_1^n \cosh \gamma_n'(b - z_o) \left(\frac{(\mu - 1)}{2} [f_1'(x_o) \right.$$

$$+ f_o'(x_o)] + \frac{K_1 K}{2} [f_1(x_o) + f_o(x_o)] \left. \right) \left. \right] - \sum_{n=o}^{\infty} \frac{2v_n \cos \frac{n\pi}{a} (a - x_o)}{a(1 + \delta_{on})}$$

$$\cdot \cos \frac{n\pi}{a} x \left[B_4^n \cosh \gamma_n' z_o \left(\frac{(\mu - 1)}{2} [f_2'(a - x_o) + f_o'(a - x_o)] \right. \right.$$

$$+ \frac{K_1 K}{2} [f_2(a - x_o) + f_o(a - x_o)] \right) + B_1^n \cosh \gamma_n'(b - z_o)$$

$$\cdot \left(\frac{(\mu - 1)}{2} [f_1'(a - x_o) + f_o'(a - x_o)] + \frac{K_1 K}{2} [f_1(a - x_o) + f_o(a - x_o)] \right) \left. \right]$$

$$\tag{4.41b}$$

and

$$f_2(x) = -\sum_{n=0}^{\infty} \frac{2v_n}{a(1 + \delta_{on})} \cos \frac{n\pi}{a} x \cosh \gamma_n'(b - z_2)(B_1^n + B_2^n)$$

$$\cdot \int_{x_o}^{a-x_o} \frac{f_2(x') - 2f_o(x') + f_1(x')}{d^2} dx' - \sum_{n=0}^{\infty} \frac{2v_n}{a(1 + \delta_{on})} \cos \frac{n\pi}{a} x_o$$

$$\cdot \cosh \gamma_n'(b - z_2) \cos \frac{n\pi}{a} x \left[B_2^n \left(\frac{(\mu - 1)}{2} [f_2'(x_o) + f_o'(x_o)] + \frac{K_1 K}{2} [f_2(x_o) \right. \right.$$

$$\left. + f_o(x_o)] \right) + B_1^n \left(\frac{(\mu - 1)}{2} [f_1'(x_o) + f_o'(x_o)] + \frac{K_1 K}{2} [f_1(x_o) + f_o(x_o)] \right) \right]$$

$$- \sum_{n=0}^{\infty} \frac{2v_n}{a(1 + \delta_{on})} \cos \frac{n\pi}{a} (a - x_o) \cosh \gamma_n'(b - z_2) \cos \frac{n\pi}{a} x$$

$$\cdot \left[B_2^n \left(\frac{(\mu - 1)}{2} [f_2'(a - x_o) + f_o'(a - x_o)] + \frac{K_1 K}{2} [f_2(a - x_o) + f_o(a - x_o)] \right) \right.$$

$$\left. + B_1^n \left(\frac{(\mu - 1)}{2} [f_1'(a - x_o) + f_o'(a - x_o)] + \frac{K_1 K}{2} [f_1(a - x_o) + f_o(a - x_o)] \right) \right]$$

$$. \quad (4.41c)$$

Equations 4.41 describe a set of three coupled equations in terms of f_1, f_o and f_2. By introducing the following functions, this set can be reduced to a set of two coupled equations which is more attractive:

$$G_v(x) = f_2(x) - 2f_o(x) + f_1(x) \qquad (4.42a)$$

and

$$G_s(x) = f_2(x) + 2f_o(x) + f_1(x) \quad . \qquad (4.42b)$$

Forming these functions gives

$$f_2(x) - 2f_0(x) + f_1(x) = -\sum_{n=0}^{\infty} \frac{2v_n}{a(1 + \delta_{on})} \cos \frac{n\pi}{a} x[(B_1^n + B_2^n) \cosh \gamma_n'$$

$$\cdot (b - z_2) + (B_3^n + B_4^n) \cosh \gamma_n' z_1 - 2B_1^n \cosh \gamma_n'(b - z_0) - 2B_4^n \cosh \gamma_n' z_0]$$

$$\cdot \left[\int_{x_0}^{a-x_0} \left(\frac{\mu - 1}{\mu_d^2} \right) [f_2(x') - 2f_0(x') + f_1(x')] \cos \frac{n\pi}{a} x' \, dx' + \cos \frac{n\pi}{a} x_0 \right.$$

$$\cdot \left(-\frac{(\mu - 1)}{4} [f_2(x_0) + 2f_0(x_0) + f_1(x_0)] - \frac{K_1 K}{4} [f_2'(x_0) + 2f_0'(x_0) \right.$$

$$\left. + f_1'(x_0)] \right) + \cos \frac{n\pi(a - x_0)}{a} \left(\frac{(\mu - 1)}{4} [f_2(a - x_0) + 2f_0(a - x_0) \right.$$

$$\left. \left. + f_1(a - x_0)] + \frac{K_1 K}{4} [f_2'(a - x_0) + 2f_0'(a - x_0) + f_1'(a - x_0)] \right) \right] \quad (4.43a)$$

and

$$f_2(x) + 2f_0(x) + f_1(x) = -\sum_{n=0}^{\infty} \frac{2v_n}{a(1 + \delta_{on})} \cos \frac{n\pi}{a} x[(B_1^n + B_2^n)$$

$$\cdot \cosh \gamma_n'(b - z_2) + (B_3^n + B_4^n) \cosh \gamma_n' z_1 + 2B_1^n \cosh \gamma_n'(b - z_0)$$

$$+ 2B_4^n \cosh \gamma_n' z_0] \left[\int_{x_0}^{a-x_0} \frac{(\mu - 1)}{\mu_d^2} [f_2(x') - 2f_0(x') + f_1'(x')] \right.$$

$$\cdot \cos \frac{n\pi}{a} x' \, dx' + \cos \frac{n\pi}{a} x_0 \left(-\frac{(\mu - 1)}{4} [f_2(x_0) + 2f_0(x_0) + f_1(x_0)] \right.$$

$$\left. -\frac{K_1 K}{4} [f_2'(x_0) + 2f_0'(x_0) + f_1'(x_0)] \right) + \cos \frac{n\pi(a - x_0)}{a} \left(\frac{(\mu - 1)}{4} \right.$$

$$\cdot [f_2(a - x_0) + 2f_0(a - x_0) + f_1(a - x_0)] + \frac{K_1 K}{4} [f_2'(a - x_0)$$

$$\left. \left. + 2f_0'(a - x_0) + f_1'(a - x_0)] \right) \right] \quad . \quad (4.43b)$$

By defining the following constants, Eqs. 4.43 simplifies greatly:

$$U^n = v_n[(B_1^n + B_2^n) \cosh \gamma_n'(b - z_2) + (B_3^n + B_4^n) \cosh \gamma_n' z_1$$

$$+ 2B_1^n \cosh \gamma_n'(b - z_0) + 2B_4^n \cosh \gamma_n' z_0] \quad ,$$

$$W^n = v_n[(B_1^n + B_2^n) \cosh \gamma_n'(b - z_2) + (B_3^n + B_4^n) \cosh \gamma_n' z_1$$

$$- 2B_1^n \cosh \gamma_n'(b - z_0) - 2B_4^n \cosh \gamma_n' z_0]$$

and

$$Q^n = \int_{x_0}^{a-x_0} \frac{\mu - 1}{\mu_d^2} G_v(x) \cos \frac{n\pi}{a} x \, dx$$

$$- \cos \frac{n\pi}{a} x_0 \left(\frac{\mu - 1}{4} G_s(x_0) + \frac{K_1 K}{4} \frac{dG_s(x_0)}{dx} \right) + \cos \frac{n\pi}{a} (a - x_0)$$

$$\cdot \left(\frac{\mu - 1}{4} G_s(a - x_0) + \frac{K_1 K}{4} \frac{dG_s(a - x_0)}{dx} \right) \quad .$$

Thus Eqs. 4.43 can be concisely stated as

$$G_v(x) = - \sum_{n=0}^{\infty} \frac{2}{a(1 + \delta_{on})} \cos \frac{n\pi}{a} x \cdot W^n Q^n \qquad (4.44a)$$

and

$$G_s(x) = - \sum_{n=0}^{\infty} \frac{2}{a(1 + \delta_{on})} \cos \frac{n\pi}{a} x \cdot U^n Q^n \quad . \qquad (4.44b)$$

The term Q^n in Eqs. 4.44 involves the first-order derivative of $G_s(x)$. The function $G_s(x)$ [obtained from $f_1(x)$, $f_0(x)$ and $f_2(x)$] is defined to be nonzero in the ferrite slab ($x_0 \leq x \leq a - x_0$) and zero everywhere outside, which means that it is discontinuous at $x = x_0$

and $x = a - x_o$ and thus its derivatives in the x-direction at the slab edges $(x_o$ or $a - x_o)$ are undefined. This problem creates difficulty in the evaluation of Q^n. To overcome this problem of discontinuity, the function $G_s(x)$ is defined only in the range $x_o \leq x \leq a - x_o$. In this manner the function $G_s(x)$ becomes differentiable at $x = x_o$ or $a - x_o$ and its approximate finite series expansion can be written as follows:

$$G_s(x) = p_o + \sum_{\ell=1}^{N_o} p_\ell \cos \frac{\ell \pi}{a - 2x_o} (x - x_o) + \sum_{\ell=1}^{N_o} q_\ell \sin \frac{\ell \pi}{a - 2x_o} (x - x_o)$$

$$x_o \leq x \leq a - x_o \quad , \quad (4.45a)$$

where p_ℓ's and q_ℓ's are arbitrary constants. Upon differentiation,

$$\frac{dG_s(x)}{dx} = - \sum_{\ell=1}^{N_o} p_\ell \frac{\ell \pi}{a - 2x_o} \sin \frac{\ell \pi}{a - 2x_o} (x - x_o) + \sum_{\ell=1}^{N_o} q_\ell \frac{\ell \pi}{a - 2x_o}$$

$$\cdot \cos \frac{\ell \pi}{a - 2x_o} (x - x_o) \quad x_o \leq x \leq a - x_o \quad , \quad (4.45b)$$

where N_o is a very large integer number. Therefore, when the series expansions for $G_s(x)$ and $[dG_s(x)/dx]$ are used, the expression for Q^n becomes

$$Q^n = \frac{\mu - 1}{\mu d^2} \int_{x_o}^{a-x_o} G_v(x) \cos \frac{n\pi}{a} x \, dx - \cos \frac{n\pi}{a} x_o \left[\frac{\mu - 1}{4} \left(p_o + \sum_{\ell=1}^{N_o} p_\ell \right) \right.$$

$$+ \frac{KK_1}{4} \sum_{\ell=1}^{N_o} \frac{\ell \pi}{a - 2x_o} q_\ell \right] + \cos \frac{n\pi}{a} (a - x_o) \left[\frac{\mu - 1}{4} \left(p_o + \sum_{\ell=1}^{o} (-1)^\ell p_\ell \right) \right.$$

$$\left. + \frac{KK_1}{4} \sum_{\ell=1}^{N_o} (-1)^\ell \frac{\ell \pi}{a - 2x_o} q_\ell \right] \quad . \quad (4.46)$$

To obtain the dispersion relation, the following procedure is undertaken: Multiplication of Eq. 4.45a by $\cos (m\pi/a)x$ and

$\sin (m\pi/a)x$ and integration in x from $x = x_0$ to $a - x_0$ yields the following linearly independent equations:

$$C_v^m + \sum_{n=0}^{\infty} \alpha_{mn} Q^n W^n = 0 \quad , \tag{4.47a}$$

$$C_s^m + \sum_{n=0}^{\infty} \alpha_{mn} Q^n U^n = 0 \tag{4.47b}$$

and

$$S_s^m + \sum_{n=0}^{\infty} \beta_{mn} Q^n U^n = 0 \quad , \tag{4.47c}$$

where

$$C_v^m = \int_{x_0}^{a-x_0} \cos \frac{m\pi}{a} x \cdot G_v(x) \, dx \quad ,$$

$$C_s^m = \int_{x_0}^{a-x_0} \cos \frac{m\pi}{a} x \cdot G_s(x) \, dx \quad ,$$

$$S_s^m = \int_{x_0}^{a-x_0} \sin \frac{m\pi}{a} x \cdot G_s(x) \, dx \quad ,$$

$$\alpha_{mn} = \frac{2}{a(1 + \delta_{on})} \int_{x_0}^{a-x_0} \cos \frac{m\pi}{a} x \cos \frac{n\pi}{a} x \, dx \quad ,$$

$$\beta_{mn} = \frac{2}{a(1 + \delta_{on})} \int_{x_0}^{a-x_0} \sin \frac{m\pi}{a} x \cos \frac{n\pi}{a} x \, dx \quad ,$$

$$n = 0,1,2,\ldots,N_0$$

and

$$m = 0,1,2,\ldots,M_0 \quad .$$

The term Q^n from Eq. 4.46 is expressed in terms of constant coefficients p_ℓ and q_ℓ, but as seen from the three linearly independent

equations (Eqs. 4.47), it is best to describe Q^n in terms of C_v^m, C_s^m and S_s^m.

To find p_ℓ's and q_ℓ's in terms C_s^m and S_s^m, Eq. 4.45a for $G_s(x)$ is multiplied by $\cos (m\pi/a)x$ and $\sin (m\pi/a)x$, respectively. The resulting equations are then integrated from $x = x_0$ to $x = a - x_0$. Thus the following two equations are obtained:

$$C_s^m = (CC)_0^m p_0 + (CC)_1^m + (CC)_2^m p_2 + \dots + (SC)_1^m q_1 + (SC)_2^m q_2 + \dots$$
$$(4.48a)$$

and

$$S_s^m = (CS)_0^m p_0 + (CS)_1^m p_1 + (CS)_2^m p_2 + \dots + (SS)_1^m q_1 + (SS)_2^m q_2 + \dots \ ,$$
$$(4.48b)$$

where

$$(CC)_n^m = \int_{x_0}^{a-x_0} \cos \frac{n\pi}{a - 2x_0} (x - x_0) \cos \frac{m\pi}{a} x \ dx \ ,$$

$$(CS)_n^m = \int_{x_0}^{a-x_0} \cos \frac{n\pi}{a - 2x_0} (x - x_0) \sin \frac{m\pi}{a} x \ dx \ ,$$

$$(SC)_n^m = \int_{x_0}^{a-x_0} \sin \frac{n\pi}{a - 2x_0} (x - x_0) \cos \frac{m\pi}{a} x \ dx \ ,$$

$$(SS)_n^m = \int_{x_0}^{a-x_0} \sin \frac{n\pi}{a - 2x_0} (x - x_0) \sin \frac{m\pi}{a} x \ dx \ ,$$

$$n = 0,1,2,\dots,N_0$$

and

$$m = 0,1,2,\dots,N_0 \ .$$

Writing Eqs. 4.48 in matrix format yields

$$
\begin{bmatrix}
C_s^o \\
C_s^1 \\
\cdot \\
\cdot \\
\cdot \\
C_s^{N_o} \\
S_s^1 \\
\cdot \\
\cdot \\
\cdot \\
S_s^{N_o}
\end{bmatrix}
= [\ H\ ] \cdot
\begin{bmatrix}
p_o \\
p_1 \\
\cdot \\
\cdot \\
\cdot \\
p_{No} \\
q_1 \\
\cdot \\
\cdot \\
\cdot \\
q_{No}
\end{bmatrix} ,
\qquad (4.49)
$$

where [H] is the coefficient matrix given by

$$
[B] =
\begin{bmatrix}
(CC)_0^0 & (CC)_1^0 & (CC)_2^0 & \cdots & (CC)_{N_0}^0 & (SC)_0^0 & (SC)_1^0 & (SC)_2^0 & \cdots & (SC)_{N_0}^0 \\
(CC)_0^1 & (CC)_1^1 & (CC)_2^1 & \cdots & (CC)_{N_0}^1 & (SC)_0^1 & (SC)_1^1 & (SC)_2^1 & \cdots & (SC)_{N_0}^1 \\
\cdot & \cdot & \cdot & \cdots & \cdot & \cdot & \cdot & \cdot & \cdots & \cdot \\
\cdot & \cdot & \cdot & \cdots & \cdot & \cdot & \cdot & \cdot & \cdots & \cdot \\
\cdot & \cdot & \cdot & \cdots & \cdot & \cdot & \cdot & \cdot & \cdots & \cdot \\
(CC)_0^{N_0} & (CC)_1^{N_0} & (CC)_2^{N_0} & \cdots & (CC)_{N_0}^{N_0} & (SC)_0^{N_0} & (SC)_1^{N_0} & (SC)_2^{N_0} & \cdots & (SC)_{N_0}^{N_0} \\
(CS)_0^1 & (CS)_1^1 & (CS)_2^1 & \cdots & (CS)_{N_0}^1 & (SS)_1^1 & (SS)_2^1 & \cdots & (SS)_{N_0}^1 \\
\cdot & \cdot & \cdot & \cdots & \cdot & \cdot & \cdot & \cdots & \cdot \\
\cdot & \cdot & \cdot & \cdots & \cdot & \cdot & \cdot & \cdots & \cdot \\
(CS)_0^{N_0} & (CS)_1^{N_0} & (CS)_2^{N_0} & \cdots & (CS)_{N_0}^{N_0} & (SS)_1^{N_0} & (SS)_2^{N_0} & \cdots & (SS)_{N_0}^{N_0}
\end{bmatrix}
$$

MICROCOPY RESOLUTION TEST CHART

NATIONAL BUREAU OF STANDARDS-1963-A

Premultiplying Eq. 4.49 by $[H]^{-1}$ and observing $[H][H]^{-1} = 1$ yields

$$
\begin{bmatrix}
p_O \\
p_1 \\
\cdot \\
\cdot \\
\cdot \\
p_{No} \\
q_1 \\
\cdot \\
\cdot \\
\cdot \\
q_{No}
\end{bmatrix}
= [\ H\ ]^{-1}
\begin{bmatrix}
C_s^O \\
C_s^1 \\
\cdot \\
\cdot \\
\cdot \\
C_s^{N_O} \\
S_s^1 \\
\cdot \\
\cdot \\
\cdot \\
S_s^{N_O}
\end{bmatrix}
. \qquad (4.50)
$$

Substitution of p_ℓ's and q_ℓ's in terms of C_s^m's and S_s^m's in Q^n of Eqs. 4.47 will produce a system of linear equations in C_v^m, C_s^m and S_s^m. To obtain a nontrivial solution for this system of linear equations requires that the large determinant $(N_O \times N_O)$ of the coefficient matrix be set to zero.

In practice the actual size of the matrix needed to obtain a reasonably accurate answer is smaller than $(N_O \times N_O)$ and it depends on the particular mode under consideration. In Chapter V Eqs. 4.47 are discussed in detail for the first-order mode $(m = 1)$ and a computer program based on a truncated matrix is written to provide numerical insight into the problem.

CHAPTER V.   COMPUTER SIMULATION AND RESULTS

5.1 Introduction

The mathematical formulations presented in Chapters III and IV were programmed on a computer and the effect of different parameters, such as slab position, width and thickness, on the dispersion characteristics and group time delay was investigated. Most of the numerical results were obtained for a fixed dc field value of $H_{dc} = 1800$ Oe and a YIG saturation magnetization of $M_o = 1750$ Oe. The tunable properties for various magnetic dc fields were also investigated and the results were presented.

As seen earlier, calculation of the dispersion relation for the purpose of root finding involves evaluation of large matrices. In Section 5.2 algorithms to find the determinant and inverse of a matrix are presented. This procedure was programmed for use in all of the determinant calculations.

Root finding of the dispersion relation is done by the Newton-Raphson method which is described in Section 5.3. A flow chart is also provided for use in programming. With the aid of this algorithm, determinant roots of the dispersion relation are found through several iterations.

In Section 5.4, the dispersion plots corresponding to the mode analysis for both parallel and normal magnetization are presented and several of its ramifications and consequences are described.

Results for the integral equation method are presented in Section 5.5. The dispersion plots and group time delay are presented and discussed for both parallel and normal magnetizations. For the normal magnetization case the analysis for the first- and zeroth-order modes and its programming are presented in detail.

5.2 Determinant Algorithm

As seen in Chapters III and IV, most of the dispersion relation equations are based on the calculation and evaluation of the determinant of the coefficient matrix. Therefore, before the roots of the dispersion relation can be found, a computational method to calculate the determinant must be developed. The following step-by-step algorithm was used to compute the determinant and/or the inverse of a matrix.[68] In this algorithm, A is the input matrix of size n x n, D is the determinant and B is the inverted matrix. To conserve storage, all stages of A are stored in the same array. The same applies to B. The steps involved are:

1. Step 1. Input and Initialization. Read ϵ,n (number of rows or columns of A) and a_{ij}; construct the identity matrix b_{ij}; set stage counter K = 1; set D = 1.0. ϵ is used for testing the matrix singularity and usually is a small number.

2. Step 2. Find pivot element (maximum magnitude element in column K on or below main diagonal); compare $|a_{KK}|$, $|a_{K+1,K}|$,...., $|a_{nK}|$ to find the largest, say $|a_{imax,K}|$. Interchange row imax of A with row K of A (same for B). If imax $\neq$ K, D = - D. Element $|a_{KK}|$ is now the largest of the set $\{|a_{KK}|, |a_{K+1}|,...., |a_{nK}|\}$.

3. Step 3. Test for near-zero maximum element (singular or near-singular matrix). If $|a_{KK}| \leqq \epsilon$ go to error exit. If $|a_{KK}| > \epsilon$ continue to Step 4.

4. Step 4. Perform stage K of reduction process:

a. Row K = (Row K/a_{KK}) and D = $a_{KK} \cdot$D. If div = a_{KK}, then $a_{Kj} = a_{Kj}$/div and $b_{Kj} = b_{Kj}$/div (j = 1, n).

b. Row i = Row i - a_{iK} Row K. If mult = a_{iK}, then $a_{ij} = a_{ij}$ - mult$\cdot a_{Kj}$ and $b_{ij} = b_{ij}$ - mult$\cdot b_{Kj}$.

5. Step 5. Test stage counter K. If K < n, set K = K + 1 and return to Step 2. If K $\geqq$ n continue to Step 6.

6. Step 6. Write output B = A^{-1} and D = $|A|$.

5.3 Newton-Raphson Method

The equation to be solved numerically is the dispersion relation, a function of frequency (f) and wave number (K), which can be written as

$$D(f,K) = 0 , \tag{5.1}$$

where D(f,K) represents the determinant of the coefficient matrix involved in the system of linear equations. Equation 5.1, in general, is a nonlinear function of f and K and can be quite complicated if the size of the matrix is large.

With the aid of the Newton-Raphson method,[69] Eq. 5.1 is solved numerically for roots K (at a known frequency f_1). The following algorithm details the exact steps used in programming Eq. 5.1 in order to find its roots:

1. Step 1. Input and Definition. Read f_1 = the frequency of operation, K_1 = the initial approximation of the root of $D(f_1,K) = 0$,

ε = the convergence term and N = the maximum number of iterations.

2. Step 2. Initialization. Set iteration counter i = 1. Set the correction term $\Delta_1 = C_1$ (C_1 is an arbitrary large positive number).

3. Step 3. Compute successive approximation of root using the Newton-Raphson iterative formula:

$$K_{i+1} = K_i - \frac{D(f_1, K_i)}{D'(f_1, K_i)} .$$

Compute the magnitude of the correction term in the current iteration

$$\Delta_{i+1} = |K_{i+1} - K_i| .$$

4. Step 4. Test for convergence or failure to converge.

a. If $\Delta_{i+1} \leq \varepsilon$ and $|D(f_1, K_{i+1})| \leq \varepsilon$, go to Step 5. If not continue.

b. If $\Delta_{i+1} > \Delta_i$, select new K_1 and return to Step 2. If $\Delta_{i+1} \leq \Delta_i$ continue.

c. If $i \leq N$, set i = i + 1 and return to Step 3. If i > N, select new K_1 and return to Step 2.

5. Step 5. Output root K_o; set $K_o = K_{i+1}$. Write K_o. Steps 1 to 5 are summarized in the flow chart shown in Fig. 5.1.

5.4 Mode Analysis Computer Simulation

In Chapter III magnetostatic-wave propagation in a waveguide partially filled with a YIG slab was analyzed. The YIG slab was in contact with the sidewalls of the waveguide. The dispersion relations for the two principal directions of magnetization were formulated.

For parallel magnetization, an exact equation for the dispersion relation was derived for a YIG slab of arbitrary thickness.

FIG. 5.1 COMPUTER PROGRAM FLOW CHART FOR EVALUATING

THE DISPERSION CHARACTERISTICS.

For normal magnetization, there is no exact solution possible. However, the dispersion relation in this case is obtained in terms of an infinite determinant that should be truncated properly. The order of truncation depends primarily on the particular mode (m) under consideration. Numerical root findings of either the exact equation or the truncated determinant on a computer are facilitated with the use of the Newton-Raphson iterative algorithm given in Section 5.3. The corresponding numerical data for the ω-k diagram and group time delay vs. frequency for parallel and normal magnetization directions are presented and discussed in the following sections.

5.4.1 Parallel Magnetization. From Eq. 3.17, several effects in terms of different device dimensions may be studied. The waveguide dimensions are assumed to be 2.0 x 1.0 cm and the slab thickness is 0.1 cm. The dispersion characteristics are plotted in Fig. 5.2. In this figure, as the YIG slab is lowered from the top to the bottom of the waveguide, the dispersion characteristics are restricted to lower propagation bandwidths. The middle positions of the slab in the upper half of the guide in some frequency ranges exhibit negative slope corresponding to negative group velocity which means energy propagates in the opposite direction to wave propagation. The corresponding group time delay in ns/cm defined by the relation $\tau_d = (\partial\omega/\partial K)^{-1}$ is shown in Fig. 5.3. From this figure, it can be seen that as the slab separation from the bottom surface is reduced, the time delay increases while the bandwidth decreases. It should be noted that these figures are drawn for the first mode and only for the forward propagating wave.

(a) $z_o = 0.95$ cm, (b) $z_o = 0.8$ cm,

(c) $z_o = 0.7$ cm, and (d) $z_o = 0.05$ cm

FIG. 5.2   EFFECT OF SLAB POSITION ON THE DISPERSION

CHARACTERISTICS.

FIG. 5.3 EFFECT OF SLAB POSITION ON GROUP TIME DELAY PER UNIT LENGTH.

Figures 5.4 and 5.5 show the effect of slab thickness on the
dispersion characteristics and group time delay per unit length.
As the slab thickness is reduced the wave propagate in a smaller
bandwidth but with a larger group delay (first mode).

Figure 5.6 shows the first- and second-order modes for
different slab positions. As can be seen, higher-order modes have
cut-off points on the K-axis and as the mode number increases, the
cut-off point also increases. Modes higher than the second are not
iown in this figure.

Tunable properties are also investigated by varying the magnetic
bias field. Figure 5.7 shows the effect of magnetic bias field on the
dispersion curves. As can be seen, the dispersion curves move up or
down the ω-k plane by varying $\overline{H}_{dc}$. Figure 5.8 shows the corresponding
effect of bias field on the time-delay characteristics.

5.4.2 Normal Magnetization. The zeroth order mode is already
discussed in Section 3.5. To obtain a nontrivial solution for higher
order modes from the system of linear equations given by Eq. 3.22,
the determinant of the coefficient matrix which is infinite in size
must be set to zero. However, for practical purposes, the matrix was
properly truncated for best accuracy. The truncation cut-off point of
the matrix depends on the mode of propagation. For example, for the
first- and second-order modes, matrices of orders up to 12 x 12 were
studied and minimum matrix size was found to be 4 x 4 and 6 x 6, respec-
tively. For higher-order modes, larger matrices must be considered.

A computer program was written, using the determinant algorithm
presented in Section 5.2, to find the determinant of the truncated
coefficient matrix. Roots of this equation are found by using the

FIG. 5.4 EFFECT OF SLAB THICKNESS ON THE DISPERSION CURVES.

FIG. 5.5 EFFECT OF SLAB THICKNESS ON GROUP TIME DELAY

PER UNIT LENGTH.

FIG. 5.6 DISPERSION CHARACTERISTICS FOR FIRST- AND
SECOND-ORDER MODE WITH SLAB POSITION AS A
PARAMETER.

FIG. 5.7 EFFECT OF MAGNETIC BIAS FIELD ON THE DISPERSION

CHARACTERISTICS.

FIG. 5.8 EFFECT OF MAGNETIC BIAS FIELD ON THE GROUP TIME DELAY CHARACTERISTICS.

Newton-Raphson method as described in Section 5.3. Through
numerical analysis it is found that the magnetostatic-wave
propagation is symmetrical in the guide cross section with respect
to the slab position. This observation was made possible by
noticing that the dispersion curves for slabs positioned in the upper
half of the guide are the same as for slabs positioned
symmetrically in the lower half of the guide. Unlike the parallel
magnetization case, the wave propagation is reciprocal for K and -K.

Figure 5.9 shows the effect of lowering the slab position.
The propagation bandwidth is reduced as can be seen from this figure.
Besides the zeroth-order mode, two higher-order modes are also
shown. These higher-order modes exist due to the finite width of
the slab. It is noted that there is a frequency cut off for
higher-order modes which increases as the mode number increases.

In Fig. 5.10, the group time delays for different modes are
plotted when the slab is placed against the top or bottom of the
guide. This figure shows the increase in time delay as the mode
number increases. Higher-order modes have higher frequency cut-
off points.

Figure 5.11 shows the effect of the slab position on the
group time delay per unit length. The slab is placed in two
positions, at the center of the guide and at the bottom or top of the
guide. The time delay increases as the slab is moved toward the
center of the guide.

Figure 5.12 shows the effect of normal magnetic field for
several bias field values. This effect on the time-delay charac-
teristics is shown in Fig. 5.13.

FIG. 5.9 EFFECT OF SLAB POSITION ON THE DISPERSION
CHARACTERISTICS.

FIG. 5.10 GROUP TIME DELAY VS. FREQUENCY FOR DIFFERENT

MODES.

FIG. 5.11 GROUP TIME DELAY VS. FREQUENCY.

FIG. 5.12 DISPERSION CHARACTERISTICS FOR VARIOUS MAGNETIC FIELDS.

FIG. 5.13 GROUP TIME DELAY CHARACTERISTICS.

5.5   Integral Equation Computer Simulation

In Chapter IV the integral equation method using Green's function was applied to the problem of magnetostatic-wave propagation in a YIG slab of finite width in a waveguide. The dispersion relations for two principal directions of magnetization were derived. These dispersion relations are in terms of infinitely large determinants as given by Eqs. 4.33 and 4.47.

To be able to solve these determinant equations on the computer, they must be properly truncated at some cut-off point. This truncation problem was studied on the computer by the method of trial and error. As a result, the trend of choosing the proper matrix size was obtained. Thus, it is found that the order of truncation depends on the particular mode under consideration (m) and the size of the air gap existing on either side of the YIG slab (x_o). Several theoretical results showing this correlation are presented.

Since parallel and normal magnetization each involve separate formulations, each case is discussed and programmed separately and the results are presented.

5.5.1   Parallel Magnetization Results.   To obtain a nontrivial unique solution for c^n's in Eq. 4.33, the infinite determinant of the coefficient matrix is set to zero in theory. However in practice, the size of the matrix is reduced by finding a proper cut-off point (N). When the determinant of the cut off (N x N) matrix is $D_N(f,K)$, the equation to be solved can be written as $D_N(f,K) = 0$.

With the aid of a computer program, results were obtained for a YIG slab against the upper surface of the waveguide with no wall gap (i.e., $x_o = 0.0$). The results are presented in Table 5.1 for

Table 5.1

Comparison of Results

Frequency f (GHz)	Exact Root K_o (cm^{-1})	$N = 8$ Approximate Root K_o' (cm^{-1})	Relative Error $[(K_o' - K_o)/K_o] \times 100$ (Percent)
7.5	$-$ 1.145	$-$ 1.147	0.1.
7.9	$-$ 2.050	$-$ 2.053	0.15
8.9	$-$ 5.379	$-$ 5.382	0.05
9.5	$-$ 9.748	$-$ 9.760	0.12
9.9	$-$ 22.843	$-$ 23.011	0.73

a = 2 cm

b = 1.0 cm

t = 0.1 cm

$\bar{H}_{dc}$ = 1800 Oe

$N = 8$ and are compared with the exact results from the earlier mode analysis. For all practical purposes, it can be seen from Table 5.1 that the percent error in all cases is less than one percent and therefore the integral equation does offer a very reliable and accurate method to calculate dispersion curves, as far as thin films are concerned.

The effect of increasing the cut-off point (N) (from 2 to 40) on the dispersion curves is shown in Fig. 5.14. From this figure it can be seen that for smaller wall gaps, a smaller matrix size is needed to produce an accurate result.

Figure 5.15 shows the relationship of the normalized wall gap $(2x_o/a)$ and the cut-off point (N). Roughly, there is an exponential increase in matrix size as the normalized wall gap $(2x_o/a)$ increases. This indicates that for narrower slabs more terms are needed to yield an accurate dispersion relation which can be verified mathematically.

The combined effect of the position and width of the YIG slab is shown in Fig. 5.16. The time delay is plotted in Fig. 5.17. It can be seen that as the slab width decreases the delay time increases and the dispersion curves bandwidth shifts downward, while as the slab position is lowered, the delay time increases and the dispersion curves are compressed with smaller bandwidths. This means that, roughly speaking, the position of the slab controls the bandwidth and its width controls the center frequency of the device. Figure 5.18 shows the effect of increasing the normalized air gap $(2x_o/a)$ on the dispersion relation. It is noted that the dispersion curves shift downward as the air gap increases. Figure 5.19 plots the wave number vs. the normalized air gap and the frequency is used as a parameter.

FIG. 5.14 RELATIONSHIP OF MATRIX SIZE AND FINAL CONVERGING VALUES.

FIG. 5.15 RELATIONSHIP OF THE WALL GAP (x_o) AND THE CUT-OFF POINT (N).

FIG. 5.16   COMBINED EFFECT OF POSITION AND WIDTH OF THE SLAB ON THE DISPERSION CURVES.

FIG. 5.17 EFFECT OF SLAB WIDTH AND POSITION ON TIME DELAY/
UNIT LENGTH.

FIG. 5.18 EFFECT OF INCREASING THE AIR GAP (x_o) ON THE DISPERSION CURVE.

FIG. 5.19 WAVE NUMBER VS. THE NORMALIZED AIR GAP.

From this figure it can be seen that an increase in frequency leads to a higher wave number (i.e., smaller wavelength) at a particular x_c. This figure also shows that at a certain frequency, wavelength does not change much as the air gap (x_g) is increased. This fact can be used in transducer design for excitation of a certain wavelength at a particular frequency.

5.5.2 Normal Magnetization Results. In Section 4.4.2 the basic formulation for magnetostatic-wave propagation for a normal bias field was derived and was given by Eqs. 4.47. In this section only the zeroth- and first-order modes are considered. Equations 4.47 are used to derive the dispersion relations in terms of the determinant of a (5 x 5) matrix. The details of this derivation are given next for more clarity.

For the first- and zeroth-order mode ($m = 0, 1$ and $n = 0, 1$) Eqs. 4.47 become

$$C_v^0 + \alpha_{00} Q^0 W^0 + \alpha_{01} Q^1 W^1 = 0 \quad , \tag{5.2a}$$

$$C_v^1 + \alpha_{10} Q^0 W^0 + \alpha_{11} Q^1 W^1 = 0 \quad , \tag{5.2b}$$

$$C_s^0 + \alpha_{00} Q^0 W^0 + \alpha_{01} Q^1 U^1 = 0 \quad , \tag{5.2c}$$

$$C_s^1 + \alpha_{10} Q^0 U^0 + \alpha_{11} Q^1 U^1 = 0 \tag{5.2d}$$

and

$$S_s^1 + \beta_{10} Q^0 U^0 + \beta_{11} Q^1 U^1 = 0 \quad , \tag{5.2e}$$

where

$$Q^0 = \frac{\mu - 1}{\mu_d^2} C_v^0 \quad , \tag{5.3a}$$

$$Q^1 = \frac{\mu - 1}{\mu d^2} C_v^1 - \cos \frac{\pi}{a} x_o \left(\frac{\mu - 1}{4} (p_o + p_1) + \frac{K^2 K_1 \pi}{4(a - 2x_o)} q_1 \right)$$

$$+ \cos \frac{\pi}{a} (a - x_o) \left(\frac{\mu - 1}{4} (p_o + p_1) - \frac{K^2 K_1 \pi}{4(a - 2x_o)} q_1 \right) \quad , \quad (5.3b)$$

$$\alpha_{oo} = 1 - 2x_o/a \quad ,$$

$$\alpha_{o1} = \frac{2}{\pi} \left(\sin \frac{\pi}{a} (a - x_o) - \sin \frac{\pi}{a} x_o \right) \quad ,$$

$$\alpha_{1o} = \frac{\alpha_{o1}}{2} \quad ,$$

$$\alpha_{11} = 1 - \frac{2x_o}{a} + \frac{1}{2\pi} \left[\sin 2\pi \left(1 - \frac{x_o}{a} \right) - \sin 2\pi \frac{x_o}{a} \right] \quad ,$$

$$\beta_{1o} = \frac{1}{\pi} \left[\cos \frac{\pi x_o}{a} - \cos \pi \left(1 - \frac{x_o}{a} \right) \right]$$

and

$$\beta_{11} = \frac{1}{2\pi} \left[\cos 2\pi \frac{x_o}{a} - \cos 2\pi \left(1 - \frac{x_o}{a} \right) \right] \quad .$$

As pointed out in Section 4.4.2, the term Q^n as given by Eq. 4.44 is in terms of p_ℓ and q_ℓ. To be able to solve Eqs. 5.2 for the dispersion relation, Q^o and Q^1 must be expressed in terms of more familiar constants C_s^o, C_s^1 and S_s^1. From Section 4.4.2, for $m = 0, 1$ and $n = 0, 1$ it follows that

$$\begin{bmatrix} p_o \\ p_1 \\ q_1 \end{bmatrix} = [H]^{-1} \begin{bmatrix} C_s^o \\ C_s^1 \\ S_s^1 \end{bmatrix} \quad , \tag{5.4}$$

where

$$
[H] = \begin{bmatrix} (CC)_0^0 & (CC)_1^0 & (SC)_1^0 \\ (CC)_0^1 & (CC)_1^1 & (SC)_1^1 \\ (CS)_0^1 & (CS)_1^1 & (SS)_1^1 \end{bmatrix} \quad , \qquad (5.5)
$$

$$
(CC)_0^0 = \int_{x_0}^{a-x_0} dx = a - 2x_0 \quad ,
$$

$$
(CC)_1^0 = \int_{x_0}^{a-x_0} \cos \frac{\pi}{a - 2x_0} (x - x_0) \, dx = 0 \quad ,
$$

$$
(CC)_0^1 = \int_{x_0}^{a-x_0} \cos \frac{\pi}{a} x \, dx = \frac{2}{\pi}\left(\sin \frac{\pi}{a} (a - x_0) - \sin \frac{\pi}{a} x_0 \right) \quad ,
$$

$$
(CC)_1^1 = \int_{x_0}^{a-x_0} \cos \frac{\pi}{a - 2x_0} (x - x_0) \cos \frac{\pi x}{a} \, dx =
$$

$$
\left\{ \frac{\frac{1}{2}}{\pi\left(\frac{1}{a} + \frac{1}{a - 2x_0}\right)} \sin\left[-\frac{\pi x_0}{a - 2x_0} + \left(\frac{\pi}{a - 2x_0} + \frac{\pi}{a}\right)x \right] + \frac{\frac{1}{2}}{\pi\left(\frac{1}{a - 2x_0} - \frac{1}{a}\right)} \right.
$$

$$
\left. \cdot \sin\left[-\frac{\pi x_0}{a - 2x_0} + \left(\frac{\pi}{a - 2x_0} - \frac{\pi}{a}\right)x \right] \right\}_{x_0}^{a-x_0} \quad ,
$$

$$
(CS)_0^1 = \int_{x_0}^{a-x_0} \sin \frac{\pi}{a} x \, dx = \frac{a}{\pi}\left[\cos \frac{\pi}{a} (a - x_0) - \cos \frac{\pi}{a} x_0 \right] \quad ,
$$

$$(CS)_1^1 = \int_{x_o}^{a-x_o} \cos \frac{\pi}{a - 2x_o} (x - x_o) \sin \frac{\pi}{a} x \, dx$$

$$= \left\{ - \frac{\frac{1}{2}}{\frac{\pi}{a} + \frac{\pi}{a - 2x_o}} \cos \left[- \frac{\pi x_o}{a-2x_o} + \left(\frac{\pi}{a - 2x_o} + \frac{\pi}{a} \right) x \right] \right.$$

$$\left. - \frac{\frac{1}{2}}{- \frac{\pi}{a - 2x_o} + \frac{\pi}{a}} \cos \left[\frac{\pi x_o}{a - 2x_o} + \left(- \frac{\pi}{a - 2x_o} + \frac{\pi}{a} \right) x \right] \right\}_{x_o}^{a-x_o} \quad ,$$

$$(SC)_1^o = \int_{x_o}^{a-x_o} \sin \frac{\pi}{a - 2x_o} (x - x_o) \, dx = \frac{2(a - 2x_o)}{\pi} \quad ,$$

$$(SC)_1^1 = \int_{x_o}^{a-x_o} \sin \frac{\pi}{a - 2x_o} (x - x_o) \cos \frac{\pi}{a} x \, dx = \left\{ - \frac{\frac{1}{2}}{\frac{\pi}{a} + \frac{\pi}{a - 2x_o}} \right.$$

$$\cdot \cos \left[- \frac{\pi x_o}{a - 2x_o} + \left(\frac{\pi}{a - 2x_o} + \frac{\pi}{a} \right) x \right] - \frac{\frac{1}{2}}{\frac{\pi}{a - 2x_o} - \frac{\pi}{a}} \cos \left[- \frac{\pi x_o}{a - 2x_o} \right.$$

$$\left. \left. + \left(\frac{\pi}{a - 2x_o} - \frac{\pi}{a} \right) x \right] \right\}_{x_o}^{a-x_o}$$

and

$$(SS)^1_1 = \int_{x_o}^{a-x_o} \sin \frac{\pi}{a - 2x_o} (x - x_o) \sin \frac{\pi}{a} x \, dx =$$

$$\left\{ \frac{\frac{1}{2}}{\frac{\pi}{a - 2x_o} - \frac{\pi}{a}} \sin \left[-\frac{\pi x_o}{a - 2x_o} + \left(\frac{\pi}{a - 2x_o} - \frac{\pi}{a} \right) x \right] + \frac{\frac{1}{2}}{\frac{\pi}{a - 2x_o} + \frac{\pi}{a}} \right.$$

$$\left. \cdot \sin \left[-\frac{\pi x_o}{a - 2x_o} + \left(\frac{\pi}{a - 2x_o} + \frac{\pi}{a} \right) x \right] \right\}_{x_o}^{a-x_o} .$$

To express p_ℓ and q_ℓ in terms of C_s^m and S_s^m, the inverse of matrix $[H]$, i.e., $[H]^{-1}$ must be known. Matrix inversion is done with the aid of a computer, so the results of this inversion are used in the following equations. To proceed with the analysis, assume $[H]^{-1}$ is known and let

$$[H]^{-1} = \begin{bmatrix} h'_{11} & h'_{12} & h'_{13} \\ h'_{21} & h'_{22} & h'_{23} \\ h'_{31} & h'_{32} & h'_{33} \end{bmatrix} . \qquad (5.6)$$

Substituting Eq. 5.6 into Eq. 5.3 for Q^1 and managing the terms yields

$$Q^1 = \frac{\mu - 1}{\mu d^2} C_v^1 + D_o C_s^0 + D_1 C_s^1 + D_2 S_s^1 , \qquad (5.7)$$

where

$$D_o = \left(-\frac{(\mu - 1)}{4}(h'_{11} + h'_{21}) - \frac{K^2 K_1 \pi}{4(a - 2x_o)} h'_{31} \right) \cos \frac{\pi}{a} x_o$$

$$+ \left(\frac{\mu - 1}{4}(h'_{11} - h'_{21}) - \frac{K^2 K_1 \pi}{4(a - 2x_o)} h'_{31} \right) \cos \frac{\pi}{a} (a - x_o) ,$$

$$D_1 = \left(-\frac{(\mu - 1)}{4}(h'_{12} + h'_{22}) - \frac{K^2 K_1 \pi}{4(a - 2x_o)} h'_{32} \right) \cos \frac{\pi}{a} x_o$$

$$+ \left(\frac{\mu - 1}{4}(h'_{12} - h'_{22}) - \frac{K^2 K_1 \pi}{4(a - 2x_o)} h'_{32} \right) \cos \frac{\pi}{a} (a - x_o)$$

and

$$D_2 = \left(-\frac{(\mu - 1)}{4}(h'_{13} + h'_{23}) - \frac{K^2 K_1 \pi}{4(a - 2x_o)} h'_{33} \right) \cos \frac{\pi}{a} x_o$$

$$+ \left(\frac{\mu - 1}{4}(h'_{13} - h'_{23}) - \frac{K^2 K_1 \pi}{4(a - 2x_o)} h'_{33} \right) \cos \frac{\pi}{a} (a - x_o) \quad .$$

Thus with the help of Eqs. 5.3a and 5.7 for Q^o and Q^1, Eqs. 5.2 in matrix notation become

$$[M(f,K)] \cdot \begin{bmatrix} C_v^o \\ C_v^1 \\ C_s^o \\ C_s^1 \\ S_s^1 \end{bmatrix} = 0 \quad , \qquad (5.8)$$

where

$$[M(f,K)] = \begin{bmatrix} 1+F\alpha_{oo}W^o & F\alpha_{o1}W^1 & D_o\alpha_{o1}W^1 & D_1\alpha_{o1}W^1 & D_2\alpha_{o1}W^1 \\ F\alpha_{1o}W^o & 1+F\alpha_{11}W^1 & D_o\alpha_{11}W^1 & D_1\alpha_{11}W^1 & D_2\alpha_{11}W^1 \\ F\alpha_{oo}U^o & F\alpha_{o1}U^1 & 1+D_o\alpha_{o1}U^1 & D_1\alpha_{o1}U^1 & D_2\alpha_{o1}U^1 \\ F\alpha_{1o}U^o & F\alpha_{11}U^1 & D_o\alpha_{11}U^1 & 1+D_1\alpha_{11}U^1 & D_2\alpha_{11}U^1 \\ F\beta_{1o}U^o & F\beta_{11}U^1 & D_o\beta_{11}U^1 & D_1\beta_{11}U^1 & 1+D_2\beta_{11}U^1 \end{bmatrix}$$

and

$$F = \frac{\mu - 1}{\mu d^2} \quad . \qquad (5.9)$$

Requiring a nontrivial unique solution yields the dispersion relation. This dispersion relation is obtained by setting the determinant of $[M(f,K)]$ to zero.

For the special case of the zeroth-order mode, the dispersion relation is given by ($m = 0$, $n = 0$):

$$1 + F\alpha_{oo} W^{o} = 0 \quad . \tag{5.10}$$

To find the dispersion relation for the first-order mode, the following equation must be solved:

$$|M(f,K)| = 0 \quad . \tag{5.11}$$

Separate computer programs were written for each mode to calculate the roots of Eqs. 5.10 and 5.11.

Figure 5.20 shows the effect of slab position in the waveguide on the dispersion characteristics. From this figure it can be seen that the effect of slab position on the dispersion curve becomes pronounced at the higher frequencies in the propagation band. Although the characteristics all converge at the lower end of the propagation band, their slopes are different. This leads to different group time delays as can be seen in Fig. 5.21. This figure shows the group time delay corresponding to Fig. 5.20. As noted in Fig. 5.21, as the slab is placed toward the center of the guide, the group time delay increases while the propagation bandwidth decreases.

Width effects on the device performance was also studied and the results are shown in Figs. 5.22 and 5.23. In Fig. 5.22, it can be seen that as the normalized air gap increases the propagation bandwidth decreases and the curves flatten out as they shift toward

FIG. 5.20 DISPERSION CURVES FOR DIFFERENT SLAB POSITIONS.

FIG. 5.21 TIME DELAY VS. FREQUENCY FOR DIFFERENT SLAB POSITIONS.

FIG. 5.22 DISPERSION CURVES FOR DIFFERENT SLAB WIDTHS.

FIG. 5.23 TIME DELAY VS. FREQUENCY FOR DIFFERENT SLAB WIDTHS.

higher frequencies. Figure 5.23 shows the corresponding group time delay vs. frequency. From this figure it can be seen that as the slab width decreases (or the air gap increases) the group time delay increases toward higher values with smaller bandwidths as noted earlier. The group time delay at smaller slab widths remains constant in a larger bandwidth and also has a higher value. This property can be used effectively in device design to obtain a constant, high group delay per unit length in a desired frequency band. Figure 5.24 plots wave number K vs. the normalized air gap $(2x_o/a)$. In this figure, the information of Fig. 5.22 is rearranged in a different fashion. It can be seen that the wave propagation at small slab widths (or large air gap) is possible only at higher frequencies with smaller wavelengths (or higher K). Once the slab width is chosen, Fig. 5.24 shows the frequency at which the device must be operated to obtain a certain wavelength, and vice versa.

Thickness effects are shown in Fig. 5.25. This figure shows that as the normalized thickness (t/b) increases the dispersion characteristics shift upward toward higher frequencies with lower propagation bandwidths. The corresponding group time delay per unit length is shown in Fig. 5.26. In this figure it is noted that as the normalized slab thickness increases from zero, the group time delay decreases and achieves its minimum value at t/b = 0.5 (i.e., when 50 percent of the guide is filled with YIG). From this point on, as the slab thickness increases, the time delay increases rapidly to high values. Although the time delay value is very high for 0.5 < t/b < 1, the available bandwidth for which the time delay is a constant value is very small and limited. On the other hand, in

FIG. 5.24 WAVE NUMBER (k) VS. NORMALIZED AIR GAP FOR

DIFFERENT FREQUENCIES.

FIG. 5.25 EFFECT OF SLAB THICKNESS ON THE DISPERSION CURVES.

FIG. 5.26 THICKNESS EFFECTS ON THE GROUP TIME DELAY AS A FUNCTION OF FREQUENCY.

the region $0 < t/b < 0.1$, the time delay approaches high values and remains constant over a large frequency range. This shows the great potential of thin films to provide constant and high values of group time delay in delay line applications with a fairly large bandwidth.

Figure 5.27 plots the initial constant group time delay vs. the normalized slab thickness. In this figure, the minimum occurs at $t/b = 0.5$ and the curve is unsymmetrical about this minimum value.

From these observations, it can be concluded that to obtain high values of group time delay over a large bandwidth, very thin slabs are required. To increase the time delay even more, it is best to choose a narrow width slab and place it in the center of the waveguide. It should be mentioned that for more accuracy, Figs. 5.25, 5.26 and 5.27 are based on the composition of results obtained from mode analysis (Eq. 3.22) for large thicknesses and integral equation formulations (Eqs. 4.47) for small thicknesses.

FIG. 5.27 INITIAL CONSTANT GROUP TIME DELAY VS. NORMALIZED
SLAB THICKNESS.

CHAPTER VI. CONCLUSIONS

6.1 Summary and Conclusions

The objective of this study was to gain a better understanding of magnetostatic-wave propagation in YIG-loaded rectangular waveguides. Both theoretical and numerical investigations were carried out to achieve this objective.

In Chapter II, the general problem of wave propagation in an unbounded ferrite medium was formulated and magnetostatic waves which propagate only in a limited range of wavelengths were identified. Next, magnetostatic-wave propagation in bounded media was studied and several important structures were analyzed. The boundary conditions that these waves should satisfy at the metal boundaries or on the slab surfaces were also introduced.

In Chapter III, magnetostatic-wave propagation in a YIG slab placed symmetrically inside a waveguide was studied. The slab had the same width as the guide and therefore a mode analysis was very useful in formulating the dispersion relations for parallel and normal magnetization. It was also shown that the obtained dispersion relations reduced to the published results for the degenerate cases when one or more of the metallic boundaries of the guide were driven to infinity.

In Chapter IV, a modified configuration was studied. In this configuration there was an equal air gap on both sides between the slab and the sidewall of the guide. The integral equation method was effectively employed to obtain the dispersion relations for two

cases of normal and parallel magnetization. The obtained dispersion relations involved infinite determinants which were properly truncated for numerical study.

In Chapter V, an extensive numerical analysis was carried out. Since most of the obtained dispersion relations were in terms of infinite determinants, the proper truncation of these determinants was studied and the results of this truncation were shown. With the help of the Newton-Raphson method the roots of the truncated determinant were found and plotted to obtain dispersion and group time-delay characteristics for both normal and parallel magnetization cases.

In conclusion, the analysis and numerical simulation carried out in this work were revealing of the magnetostatic-wave behavior in a ferrite-loaded waveguide. The width, thickness, and position of the slab were shown to be a determining factor in the device performance. The following conclusions can be stated briefly:

1. For parallel magnetization, to obtain high time-delay values, the YIG slab must be thin, narrow and placed at the bottom of the guide. On the other hand, to maximize the device bandwidth, a thick, narrow YIG slab positioned at the top of the guide is preferred.

2. For normal magnetization, to achieve high values of time delay, again a thin, narrow slab must be used. This time it should be placed in the center of the guide. On the other hand, high bandwidths can be obtained by using wide, thin slabs placed at the top or bottom of the guide.

It is noted that there exists a trade-off between the time delay and the device bandwidth, and maximization of one property

leads to a poor value in the other. Thus some design compromises should be made.

In general, based on the presented analysis in the previous chapters and certain design specifications, an optimum device geometry can be designed to provide the best device performance over a desired frequency range.

6.2 Suggestions for Further Study

The formulation developed in this investigation for two principal directions of magnetization provides good simulation results and insight into the device performance. However, there are several additional topics that would help to realize the full potential of magnetostatic-wave devices and thus need further study. They are:

1. A study of magnetostatic-wave propagation in a waveguide in the presence of (a) a magnetic bias field in the transverse plane at an angle θ_o to the slab plane and (b) an axial magnetization.

2. An analysis and proper modeling of the propagation losses.

3. An analysis of magnetostatic-wave propagation in a thick YIG slab in a waveguide $(x_o \neq 0)$.

4. The design and fabrication of the devices and experimental studies of the magnetostatic-wave propagation properties and comparison with the theoretical results.

5. A study of the higher-order modes for signal processing applications.

APPENDIX A.   SAMPLE COMPUTER PROGRAMS

The following sample programs in FORTRAN are written to

solve for roots (K) of the function G(K,JMODE,U,K1) by using the

Newton-Raphson method.   The function G(K,JMODE,U,K1) represents

the determinant of the truncated coefficient matrix.   These programs

are based on the determinant calculation procedure and the Newton-

Raphson iterative method as described in Chapter V.   The most

important symbols used in this program are defined as follows:

A	Waveguide width in cm.
B	Waveguide height in cm.
D	One half of the slab thickness in cm.
FRQ	Operating frequency in GHz.
HI	Internal dc magnetic field in Oe.
JMODE	The specific mode under consideration.
K	Wave number in cm^{-1}.
K1	Off-diagonal term of the permeability tensor.
LN	Size of the truncated matrix.
MS	Magnetization saturation in Oe.
XKX	The initial value of K to start the iteration.
XO	Gap length in cm.
U	Diagonal term of the permeability tensor.
ZO	Position of the slab in the waveguide in cm.

The first sample program finds the roots of the dispersion

relation as given by the coefficient matrix of Eq. 4.84, where H_{dc}

is in the x-direction.   This program consists of the following parts:

1. Main program--finds the roots of function G by using the Newton-Raphson method.

2. Function G(K,JMODE,U,K1)--constructs and loads the truncated matrix. This function subprogram takes as its input the wave number (K), the specific mode under study (JMODE), and the operating frequency (U,K1) and returns the determinant of the truncated matrix in G by calling function XDET(A,N).

3. Function XDET(A,N)--computes the determinant of the N by N truncated matrix A and returns the value of the determinant in XDET.

```
C....................PROGRAM #1............................
C.......PROGRAM TO CALCULATE ROOTS WHEN X0 IS NOT ZERO AND
C.......Hdc IS PARALLEL TO THE SLAB PLANE, i.e., Hdc=H0.X
C.......THIS PROGRAM CALCULATES ROOTS OF THE ODD MODES ONLY.
C
C                         ***
C.......THIS IS THE MAIN PROGRAM IN  FORTRAN
C.......WRITTEN TO SOLVE FOR ROOTS (K) OF THE NONLINEAR
C.......EQUATION G(FRQ,K)=0 USING THE NEWTON-RAPHSON METHOD,
C.......WHERE FREQUENCY(FRQ) IS A KNOWN VALUE.
        IMPLICIT REAL*4 (K,M)
        DIMENSION DELTA(15),K(15)
        COMMON A,B,D,Z0,X0,LN
        EPS=.5
        DK=.1
        NITER=5
        DELTA(1)=100000.
        KX=-1.
        DO 300 NR=1,5
C.......INPUT STATEMENT TO SET THE VALUES  OF FREQUENCY(FRQ),
C.......INITIAL WAVE NUMBER(XKX),GAP LENGTH(X0),MATRIX SIZE
C.......(LN=5),SLAB POSITION(Z0),WAVEGUIDE WIDTH(A),WAVEGUIDE
C.......HEIGHT(B),ONE HALF SLAB THICKNESS(D),SATURATION
C.......MAGNETIZATION(MS),INTERNAL DC MAGNETIC FIELD(HI) AND
C.......MODE UNDER STUDY(JMODE).
        NAMELIST/RAD/FRQ,XKX, X0,LN,Z0,A,B,D,MS,HI,JMODE
        READ (5,RAD)
        WRITE(6,RAD)
201     FORMAT(F10.3,I2)
        K(1)=XKX
90      FORMAT(//3X,3F20.3)
93      FORMAT(I2.3F10.3)
91      FORMAT(2F10.3)
        FRQ0=2.8*HI/1000.
        FRQM=2.8*MS/1000.
        DEL=FRQ0**2-FRQ**2
        K1=FRQ*FRQM/DEL
        U=1.+K1*FRQ0/FRQ
        WRITE(6,90) U,D,Z0
C.......ROOT FINDING BY ITERATIVE STEPS
```

```
96        DO 200 I=1,NITER
          I1=I+1
          XKDK=K(I)+DK
          XV=G(XKDK,JMODE,U,K1)
          XW=G(K(I),JMODE,U,K1)
          GPRIM=(XV-XW)/DK
          WRITE(6,90) GPRIM,XV,XW
          K(I1)=K(I)-XW/GPRIM
          DIFF=K(I1)-K(I)
          DELTA(I1)=ABS(DIFF)
          XX=G(K(I1),JMODE,U,K1)
          IF (DELTA(I1) .LE. EPS) GO TO 98
92        IF(DELTA(I1) .LE. DELTA(I)) GO TO 95
          GO TO 97
98        IF (ABS(XX) .LE. EPS) GO TO 100
          GO TO 92
97        WRITE(6,90)   K(I),DELTA(I),DELTA(I1)
          K(1)=K(1)+KX
          WRITE(6,89) K(1)
89        FORMAT(3X,'K(1) IS RESET TO A NEW VALUE:',F9.2)
          GO TO 96
99        WRITE (6,94) I,K(I1),DELTA(I1),XX
200       CONTINUE
100       WRITE (6,94) I, K(I1),DELTA(I1),XX
94        FORMAT(I2,2F10.3,F20.3)
300       CONTINUE
          STOP
          END
C.......FUNCTION G(F,K) DESCRIBES THE DETERMINANT OF AN
C.......N BY N TRUNCATED MATRIX.THE VALUE OF THE GAP
C.......LENGTH(X0) IS NOT ZERO AND Hdc=H0.X.
          FUNCTION G(K,JMODE,U,K1)
          IMPLICIT REAL(K)
          DIMENSION XM(40,40,2,2),G1(40,2,2),BIG(40,40),BETA(40,40),
     1    II(40),JJ(40)
          COMMON   A,B,D,Z0,X0,LN
200       FORMAT(2X,'X0=',F7.3,'   LN=',I2)
          X0A=X0/A
          Z1=Z0-D
          Z2=Z0+D
          PI=3.1416
          S1=B-Z1
          S2=B-Z2
          DO 10 I=1,LN,2
          DO 20 J=1,LN,2
          ALFA=J*PI/A
          ALFA2=ALFA*ALFA
          GAMA=SQRT(ALFA2+K*K)
          V=1.0/(GAMA*SINH(GAMA*B))
          P2=-(U-1.)*(ALFA2)/(2*D*GAMA*GAMA)
          P1=-K1*K-P2
          P3=(U-1.)*K*K/GAMA
          P4=-P2+K1*K
          CZ1=COSH(GAMA*Z1)
          CZ2=COSH(GAMA*Z2)
          CS1=COSH(GAMA*S1)
          CS2=COSH(GAMA*S2)
          G1(J,1,1)=V*CZ1*(P4*CS1+P2*CS2+P3*SINH(GAMA*S1))
          G1(J,1,2)=V*CZ1*(P1*CS2+P2*CS1-P3*SINH(GAMA*S2))
          G1(J,2,1)=V*CS2*(P4*CZ1+P2*CZ2-P3*SINH(GAMA*Z1))
          G1(J,2,2)=V*CS2*(P1*CZ2+P2*CZ1+P3*SINH(GAMA*Z2))
          DO 30 L2=1,2
          DO 40 L=1,2
          IF (I .EQ. J) GO TO 50
          IJ1=I-J
          IJ2=I+J
          A1=IJ1*PI*X0A
          A2=IJ2*PI*X0A
          BETA(I,J)=-.63662*((SIN(A1)/IJ1)+(SIN(A2)/IJ2))
          XM(I,J,L2,L)=BETA(I,J)*G1(J,L2,L)
          GO TO 40
```

```
50        A3=2*I*PI*X0A
          BETA(I,I)=1.-2*X0A-SIN(A3)/(I*PI)
          XM(I,I,L2,L)=BETA(I,I)*G1(I,L2,L)
40        CONTINUE
30          CONTINUE
20            CONTINUE
10              CONTINUE
C........LOADING THE BIG MATRIX
          DO 60 I=1,2
          DO 60 J=1,2
          DO 55 L=1,LN,2
          II(L)=I+L-1
          JJ(L)=J+L-1
55        CONTINUE
          DO 56 L2=1,LN,2
          DO 57 L3=1,LN,2
          BIG(II(L2),JJ(L3))=XM(L2,L3,I,J)
57        CONTINUE
56          CONTINUE
60            CONTINUE
          LN1=LN+1
          DO 70 I=1,LN1
70        BIG(I,I)=BIG(I,I)+1.0
          G=XDET(BIG,LN1)
          RETURN
          END
C.......FUNCTION SUBPROGRAM TO CALCULATE THE DETERMINANT
C.......OF AN N BY N MATRIX A.
          FUNCTION XDET(A,N)
          DIMENSION A(40,40),B(40,40)
          EPS=.00001
C......CONSTRUCT IDENTITY MATRIX
          DO 6 I=1,N
          DO 5 J=1,N
          IF (I-J) 4,3,4
3         B(I,J)=1.
          GO TO 5
4         B(I,J)=0.0
5         CONTINUE
6           CONTINUE
C......LOCATE MAXIMUM MAGNITUDE A(I,K) ON OR BELOW MAIN
C.......DIAGONAL
          DEL=1.0
          DO 45 K=1,N
          IF (K-N) 12,30,30
12        IMAX=K
          AMAX=ABS(A(K,K))
          KP1=K+1
          DO 20 I=KP1,N
          IF (AMAX-ABS(A(I,K))) 15,20,20
15        IMAX=I
          AMAX=ABS(A(I,K))
20        CONTINUE
C......INTERCHANGE ROWS  IMAX AND K IF IMAX NOT EQUAL TO K
          IF (IMAX-K) 25,30,25
25        DO 29 J=1,N
          ATMP=A(IMAX,J)
          A(IMAX,J)=A(K,J)
          A(K,J)=ATMP
          BTMP=B(IMAX,J)
          B(IMAX,J)=B(K,J)
29        B(K,J)=BTMP
          DEL=-DEL
30        CONTINUE
          IF (ABS(A(K,K))-EPS) 93,93,35
C......TEST FOR SINGULAR MATRIX
35        DEL=A(K,K)*DEL
C......DIVIDE PIVOT ROW BY ITS MAIN DIAGONAL ELEMENT
          DIV=A(K,K)
          DO 38 J=1,N
          A(K,J)=A(K,J)/DIV
38        B(K,J)=B(K,J)/DIV
C......REPLACE EACH ROW BY LINEAR COMBINATION WITH PIVOT ROW
```

```
          DO 43 I=1,N
          AMULT=A(I,K)
          IF(I-K) 39,43,39
39        DO 42 J=1,N
          A(I,J)=A(I,J)-AMULT*A(K,J)
42        B(I,J)=B(I,J)-AMULT*B(K,J)
43        CONTINUE
45        CONTINUE
          XDET=DEL
99        RETURN
93        GO TO 99
          END
```

The second sample program finds the roots of the dispersion

relation for zeroth- and first-order modes as described by a 5 by 5

matrix given by Eq. 5.10 where H_{dc} is in the z-direction. This

program has the following parts:

1. Main program--finds the roots of function G.

2. Function $G(K,JMODE,U,K1)$--constructs and loads the

truncated 5 by 5 matrix. This function subprogram takes as its

input the wave number (K), the specific mode under study (JMODE), and

the operating frequency (U,K1) and returns the determinant of the

truncated matrix in G by calling subroutine XINV(A,B,XDET,N).

3. Subroutine XINV(A,B,XDET,N)--computes the inverse of the

N by N truncated matrix A and returns it in matrix B. This

subroutine also computes the determinant of matrix A and returns

it in XDET.

```
C.....................PROGRAM #2.......................
C.......PROGRAM TO CALCULATE ROOTS WHEN X0 IS NOT ZERO AND
C.......Hdc IS NORMAL TO THE SLAB,i.e., Hdc=H0.Z
C.......THIS PROGRAM CALCULATES ROOTS OF THE FIRST MODE ONLY.

C                       ***
C.......THIS IS THE MAIN PROGRAM WRITTEN IN FORTRAN SOLVING
C.......FOR ROOTS (K) OF THE NONLINEAR EQUATION G(FRQ,K)=0.
C.......USING THE NEWTON-RAPHSON METHOD, WHERE FRQ IS KNOWN.
          IMPLICIT REAL*4 (K,M)
          DIMENSION DELTA(15),K(15)
          COMMON A,B,D,Z0,X0,LN,MS,HI
          EPS=.5
          DK=.1
          NITER=5
          DELTA(1)=100000.
          KX=-1.
          DO 300 NR=1,5
```

```
C.......INPUT STATEMENT TO SET THE VALUES  OF FREQUENCY(FRQ),
C.......INITIAL WAVE NUMBER(XKX),GAP LENGTH(X0),MATRIX SIZE
C.......(LN=5),SLAB POSITION(Z0),WAVEGUIDE WIDTH(A),WAVEGUIDE
C.......HEIGHT(B),ONE HALF SLAB THICKNESS(D),SATURATION
C.......MAGNETIZATION(MS),INTERNAL DC MAGNETIC FIELD(HI),MODE
C.......UNDER STUDY(JMODE).
        NAMELIST/RAD/FRQ,XKX, X0,LN,Z0,A,B,D,MS,HI,JMODE
        READ (5,RAD)
        WRITE(6,RAD)
201     FORMAT(F10.3,I2)
        K(1)=XKX
90      FORMAT (//3X,3F20.3)
93      FORMAT(I2,3F10.3)
91      FORMAT(2F10.3)
        FRQ0=2.8*HI/1000.
        FRQM=2.8*MS/1000.
        DEL=FRQ0**2-FRQ**2
        K1=FRQ*FRQM/DEL
        U=1.+K1*FRQ0/FRQ
        WRITE(6,90) U,K1,Z0
C.......ROOT FINDING  BY ITERATIVE STEPS
96      DO 200 I=1,NITER
        I1=I+1
        XKDK=K(I)+DK
        XV=G(XKDK,JMODE,U,K1)
        XW=G(K(I),JMODE,U,K1)
        GPRIM=(XV-XW)/DK
        WRITE(6,90) GPRIM,XV,XW
        K(I1)=K(I)-XW/GPRIM
        DIFF=K(I1)-K(I)
        DELTA(I1)=ABS(DIFF)
        XX=G(K(I1),JMODE,U,K1)
        IF (DELTA(I1) .LE. EPS) GO TO 98
92      IF(DELTA(I1) .LE. DELTA(I)) GO TO 99
        GO TO 97
98      IF (ABS(XX) .LE. EPS) GO TO 100
        GO TO 92
97      WRITE(6,90)   K(I),DELTA(I),DELTA(I1)
        K(1)=K(1)+KX
        WRITE(6,89) K(1)
89      FORMAT(3X,'K(1) IS RESET TO A NEW VALUE:',F9.2)
        GO TO 96
99      WRITE (6,94) I,K(I1),DELTA(I1),XX
200     CONTINUE
100     WRITE (6,94) I, K(I1),DELTA(I1),XX
94      FORMAT(I2,2F10.3,F20.3)
300     CONTINUE
        STOP
        END
C.......FUNCTION G(F,K) DESCRIBES THE DETERMINANT OF A
C.......5 BY 5 MATRIX FOR THE FIRST-ORDER MODE, WHEN
C.......Hdc=H0.Z AND X0 IS NOT EQUAL TO ZERO.
        FUNCTION G(K,JMODE,U,K1)
        IMPLICIT REAL(K)
        DIMENSION XA(40,40),XB(40,40),VN(2),UN(2),BIG(40,40)
        COMMON A,B,D,Z0,X0,LN,MS,HI
        Z1=Z0-D
        Z2=Z0+D
        PI=3.1416
        BZ0=B-Z0
        BZ1=B-Z1
        BZ2=B-Z2
        X0A=X0/A
        AX0=A-X0
        A2X0=A-2*X0
        A0=-PI*X0/A2X0
        A1=-2*A0/A
        A2=2*PI*(1-X0A)/A2X0
        PA2=PI*AX0/A
        PA1=PI*X0A
        A3=A0+A2*AX0
```

```
            A4=A0+A2*X0
            A5=A0+A1*AX0
            A6=A0+A1*X0
            S34=.5*(SIN(A3)-SIN(A4))/A2
            S56=.5*(SIN(A5)-SIN(A6))/A1
            C34=.5*(-COS(A3)+COS(A4))/A2
            C56=.5*(-COS(A5)+COS(A6))/A1
            XA(1,1)=A2X0
            XA(1,2)=0.
            XA(1,3)=2*A2X0/PI
            XA(2,1)=.318*A*(SIN(PA2)-SIN(PA1))
            XA(2,2)=S34+S56
            XA(2,3)=C34+C56
            XA(3,1)=.318*A*(COS(PA2)-COS(PA1))
            XA(3,2)=C34-C56
            XA(3,3)=S34-S56
            NN=3
            CALL XINV(XA,XB,XDET,NN)
            DO 10 I=1,2
            II=I-1
            ALFA=II*PI/A
            ALFA2=ALFA*ALFA
            GAMA=SQRT(ALFA2+K*K)
            W=1.0/(GAMA*SINH(GAMA*B))
            F=(U-1.)/(U*D*D)
            SZ0=SINH(GAMA*Z0)
            SZ1=SINH(GAMA*Z1)
            SZ2=SINH(GAMA*Z2)
            SBZ0=SINH(GAMA*BZ0)
            SBZ1=SINH(GAMA*BZ1)
            SBZ2=SINH(GAMA*BZ2)
            CZ0=COSH(GAMA*Z0)
            CZ1=COSH(GAMA*Z1)
            CBZ0=COSH(GAMA*BZ0)
            CBZ2=COSH(GAMA*BZ2)
            B1=(SZ0-SZ1)/GAMA
            B2=(SZ2-SZ0)/GAMA
            B3=(-SBZ0+SBZ1)/GAMA
            B4=(-SBZ2+SBZ0)/GAMA
            VN(I)=W*((B1+B2)*CBZ2+(B3+B4)*CZ1-2*B1*CBZ0-2*B4*CZ0)
            UN(I)=VN(I)+4*W*B1*CBZ0+4*W*B4*CZ0
10          CONTINUE
            CC1=COS(PA1)
            CC2=COS(PA2)
            DC0=-.25*(K*K*K1*PI)*(CC1+CC2)/A2X0
            U14=(U-1)/4
            DC1=U14*(XB(1,1)+XB(2,1))
            DC2=U14*(XB(1,1)-XB(2,1))
            DC3=U14*(XB(1,2)+XB(2,2))
            DC4=U14*(XB(1,2)-XB(2,2))
            DC5=U14*(XB(1,3)+XB(2,3))
            DC6=U14*(XB(1,3)-XB(2,3))
            D0=-DC1*CC1+DC2*CC2+DC0*XB(3,1)
            D1=-DC3*CC1+DC4*CC2+DC0*XB(3,2)
            D2=-DC5*CC1+DC6*CC2+DC0*XB(3,3)
            A00=1.-2*X0A
            A01=.6366*(SIN(PA2)-SIN(PA1))
            A10=A01/2.
            A11=A00+.159*(SIN(2*PA2)-SIN(2*PA1))
            B10=.318*(COS(PA1)-COS(PA2))
            B11=.159*(COS(2*PA1)-COS(2*PA2))
            AV0=A01*VN(2)
            AV1=A11*VN(2)
            AU0=A01*UN(2)
            AU1=A11*UN(2)
            BU1=B11*UN(2)
C.......LOADING THE MATRIX IN THE FINAL FORM READY
C.......FOR DETERMINANT CALCULATION.
            BIG(1,1)=1.+F*A00*VN(1)
            BIG(1,2)=F*AV0
            BIG(1,3)=D0*AV0
            BIG(1,4)=D1*AV0
            BIG(1,5)=D2*AV0
            BIG(2,1)=F*A10*VN(1)
```

```
                   BIG(2,2)=1.+F*AV1
                   BIG(2,3)=D0*AV1
                   BIG(2,4)=D1*AV1
                   BIG(2,5)=D2*AV1
                   BIG(3,1)=F*A00*UN(1)
                   BIG(3,2)=F*AU0
                   BIG(3,3)=1.+D0*AU0
                   BIG(3,4)=D1*AU0
                   BIG(3,5)=D2*AU0
                   BIG(4,1)=F*A10*UN(1)
                   BIG(4,2)=F*AU1
                   BIG(4,3)=D0*AU1
                   BIG(4,4)=1.+D1*AU1
                   BIG(4,5)=D2*AU1
                   BIG(5,1)=F*B10*UN(1)
                   BIG(5,2)=F*BU1
                   BIG(5,3)=D0*BU1
                   BIG(5,4)=D1*BU1
                   BIG(5,5)=1.+D2*BU1
                   LN=5
                   CALL XINV(BIG,XB,XDET,LN)
                   G=XDET
                   RETURN
                   END
C......SUBROUTINE FOR DETERMINANT CALCULATION AND
C......MATRIX INVERSION BY ELIMINATION WITH
C......PARTIAL PIVOTING.
                   SUBROUTINE XINV(A,B,XDET,N)
C......A=ORIGINAL MATRIX, B=IVERSE MATRIX, XDET=
C......DETERMINANT, N=MATRIX SIZE.
                   DIMENSION A(40,40),B(40,40)
                   EPS=.00001
C......CONSTRUCT IDENTITY MATRIX B(I,J)=1

                   DO 6 I=1,N
                   DO 5 J=1,N
                   IF (I-J) 4,3,4
3                  B(I,J)=1.
                   GO TO 5
4                  B(I,J)=0.0
5                  CONTINUE
6                  CONTINUE
C......LOCATE MAXIMUM MAGNITUDE A(I,K) ON OR BELOW MAIN
C......DIAGONAL
                   DEL=1.0
                   DO 45 K=1,N
                   IF (K-N) 12,30,30
12                 IMAX=K
                   AMAX=ABS(A(K,K))
                   KP1=K+1
                   DO 20 I=KP1,N
                   IF (AMAX-ABS(A(I,K))) 15,20,20
15                 IMAX=I
                   AMAX=ABS(A(I,K))
20                 CONTINUE
C......INTERCHANGE ROWS IMAX AND K IF IMAX NOT EQUAL TO K
                   IF (IMAX-K) 25,30,25
25                 DO 29 J=1,N
                   ATMP=A(IMAX,J)
                   A(IMAX,J)=A(K,J)
                   A(K,J)=ATMP
                   BTMP=B(IMAX,J)
                   B(IMAX,J)=B(K,J)
29                 B(K,J)=BTMP
                   DEL=-DEL
30                 CONTINUE
                   IF (ABS(A(K,K))-EPS) 93,93,35
C......TEST FOR SINGULAR MATRIX
35                 DEL=A(K,K)*DEL
```

```
C.......DIVIDE PIVOT ROW BY ITS MAIN DIAGONAL ELEMENT
        DIV=A(K,K)
        DO 38 J=1,N
        A(K,J)=A(K,J)/DIV
38      B(K,J)=B(K,J)/DIV
C.......REPLACE EACH ROW BY LINEAR COMBINATION WITH PIVOT ROW
        DO 43 I=1,N
        AMULT=A(I,K)
        IF(I-K) 39,43,39
39      DO 42 J=1,N
        A(I,J)=A(I,J)-AMULT*A(K,J)
42      B(I,J)=B(I,J)-AMULT*B(K,J)
43      CONTINUE
45      CONTINUE
        XDET=DEL
99      RETURN
93      GO TO 99
        END
```

LIST OF REFERENCES

1. Stiglitz, M. R. and Sethares, J. C., "Magnetostatic Waves Take Over Where SAWs Leave Off," _Microwave J._, vol. 25 No. 2, pp. 18-111, February 1982.

2. Owens, J. M., Carter, R. L. and Smith, C. V., Jr., "Magneto-static Waves, Microwave SAW?" _1980 IEEE Ultrasonic Symp. Proc._, Boston, MA, pp. 506-512, November 1980.

3. Collins, J. H., Owens, J. M. and Smith, C. V., Jr., "Magneto-static Wave Signal Processing," _1977 Ultrasonic Symp. Proc._, Phoenix, AZ, pp. 541-552, October 1977.

4. Morgenthaler, F. R., "MW Signal Processing with Magnetostatic Waves and Modes," _Microwave J._, vol. 25, No. 2, pp. 83-90, February 1982.

5. Adam, J. D., Daniel, M. R. and O'Keeffe, T. W., "Magnetostatic Wave Devices," _Microwave J._, vol. 25, No. 2, pp. 95-99, February 1982.

6. Vittoria, C. and Wilsey, N. D., "Magnetostatic Wave Propagation Losses in an Anisotropic Insulator," _J. Appl. Phys._, vol. 45, No. 1, pp. 414-420, January 1974.

7. Sethares, J. C. and Stiglitz, M. R., "Propagation Loss and MSSW Delay Lines," _IEEE Trans. on Magnetics_, vol. MAG-10, No. 3, pp. 787-790, September 1974.

8. Vittoria, C., Webb, D., Lubitz, P. and Lessoff, H., "Magneto-static Propagation Loss in Thin Films of Liquid Phase Epitaxy YIG," _IEEE Trans. on Magnetics_, vol. MAG-11, No. 5, pp. 1259-1261, September 1975.

9. Adams, J. D., Collins, J. H. and Owens, J. M., "Microwave Device Applications of Epitaxial Magnetic Garnets," _The Radio and Electronic Engineer_, vol. 45, No. 12, pp. 738-748, December 1975.

10. Sethares, J. C., "Magnetostatic Wave Devices and Applications," _J. Appl. Phys._, vol. 53, No. 3, pp. 2646-2651, March 1982.

11. Tiernan, R. J. and Schloemann, E., "Nonreciprocal Delay Line for Use in S-Band Tubes," _IEEE Trans. on Microwave Theory and Techniques_, vol. MTT-23, No. 10, pp. 813-818, October 1975.

12. Haworth, J., "A Magnetostatic Delay Line Oscillator," _1975 IEEE-MTT-S Int. Microwave Symp. Digest_, Palo Alto, CA, pp. 371-372, May 1975.

13. Miller, N.D.J. and Brown, D., "Tunable Magnetostatic Surface Wave Oscillator," _Electronics Letters_, vol. 12, No. 9, pp. 209-210, April 1976.

14. Adam, J. D., Bardai, Z. M., Collins, J. H. and Owens, J. M., "Tapped Microwave Nondispersive Magnetostatic Delay Lines," _AIP Conf. Proc._, San Francisco, CA, No. 24, pp. 499-500, December 1974.

15. Bongianni, W. L., "X-Band Signal Processing Using Magnetic Waves," _Microwave J._, vol. 17, No. 1, p. 49, January 1974.

16. Adam, J. D., Owens, J. M. and Collins, J. H., "Magnetostatic Delay Lines for Group Delay Equalisation in Millimetric Wave-guide Communication Systems," _IEEE Trans. on Magnetics_, vol. MAG-10, No. 3, pp. 783-786, September 1974.

17. Bardai, Z. M., Adam, J. D., Collins, J. H. and Parekh, J. P., "Delay Lines Based on Magnetostatic Volume Waves in Epitaxial YIG," _AIP Conf._, Pittsburgh, PA, No. 34, pp. 268-270, June 1976.

18. Brinlee, W. R., Owens, J. M., Smith, C. V., Jr., and Carter, R. L., "'Two-Port' Magnetostatic Wave Resonators Utilizing Periodic Metal Reflective Arrays," _J. Appl. Phys._, vol. 52, No. 3, pp. 2276-2278, March 1981.

19. Daniel, M. R., Adam, J. D., and O'Keeffe, T. W., "A Linearly Dispersive Magnetostatic Delay Line at X-Band," _IEEE Trans. on Magnetics_, vol. MAG-15, No. 6, pp. 1735-1737, November 1979.

20. Ganguly, A. K. and Webb, D. C., "Microstrip Excitation of Magnetostatic Surface Waves: Theory and Experiment," _IEEE Trans. on Microwave Theory and Techniques_, vol. MTT-23, No. 12, pp. 998-1006, December 1975.

21. Ganguly, A. K., Webb, D. C. and Banks, C., "Complex Radiation Impedance of Microstrip-Excited Magnetostatic-Surface Waves," _IEEE Trans. on Microwave Theory and Techniques_, vol. MTT-26, No. 6, pp. 444-447, June 1978.

22. Parekh, J. P. and Tuan, H. S., "Meander Line Excitation of Magnetostatic Surface Waves," _Proc. IEEE_, vol. 67, No. 1, pp. 182-183, January 1979.

23. Schilz, W., "Spin-Wave Propagation in Epitaxial YIG Films," Philips Research Report No. 28, Philips Industries, N. V. Philips, Eindhoven, The Netherlands, pp. 332-335, 1973.

24. Collins, J. H. and Pizzarello, F. A., "Propagating Magnetic Waves in Thick Films. A Complementary Technology to Surface Wave Acoustics," _Int. J. Electronics_, vol. 34, No. 31, pp. 319-351, March 1973.

25. Adam, J. D., Patterson, R. W. and O'Keefe, T. W., "Magnetostatic Wave Transducers," J. Appl. Phys., vol. 49, No. 3, Part 2, pp. 1797-1799, March 1978.

26. Wu, H. J., Smith, C. V., Jr., Collins, J. H. and Owens, J. M., "Bandpass Filtering with Multibar Magnetostatic-Surface-Wave Microstrip Transducers," Electronic Letters, vol. 13, No. 20, pp. 610-611, September 1977.

27. Sethares, J. C. and Weinberg, I. J., "Apodization of Variable Coupling MSSW Transducers," J. Appl. Phys., vol. 50, No. 3, pp. 2458-2460, March 1979.

28. Owens, J. M., Carter, R. L., Smith, C. V., Jr., and Hasnian, G., "A 3-Port Model for Magnetostatic Wave Transducers," 1980 IEEE Ultrasonic Symp. Proc., Boston, MA, pp. 506-512, November 1980.

29. Wu, H. J., "Magnetostatic Wave Transducers," Ph.D. Dissertation, The University of Texas at Arlington, 1978.

30. Wu, H. J., Smith, C. V., Jr., and Owens, J. M., "Bandpass Filtering and Input Impedance Characterization for Driven Multielement Transducer Pair-Delay Line Magnetostatic Wave Devices," J. Appl. Phys., vol. 50, No. 3, pp. 2455-2457, March 1979.

31. Volluet, G., "Unidirectional Magnetostatic Forward Volume Wave Transducers," IEEE Trans. on Magnetics, vol. MAG-16, No. 5, pp. 1162-1164, September 1980.

32. Emtage, P. R., "Interaction of Magnetostatic Waves with a Current," J. Appl. Phys., vol. 49, No. 8, pp. 4475-4485, August 1978.

33. Parekh, J. P. and Tuan, H. S., "Excitation of Magnetostatic Backward Volume Waves," IEEE Trans. on Magnetics, vol. MAG-16, No. 5, pp. 1165-1167, September 1980.

34. Parekh, J. P., "Theory for Magnetostatic Forward Volume Wave Excitation," J. Appl. Phys., vol. 50, No. 3, pp. 2452-2454, March 1979.

35. Young, P., "Efficient Broadband Excitation of the n=0 Surface Magnetostatic Waves in a YIG Slab," Electronics Letters, vol. 4, No. 25, pp. 566-568, December 1968.

36. Damon, R. W. and Eshbach, J. R., "Magnetostatic Modes of a Ferrimagnetic Slab," J. Phys. Chem. Solids, vol. 19, No. 3/4, pp. 308-320, May 1961.

37. Tsai, M. C., Wu, H. J., Owens, J. M. and Smith, C. V., Jr., "Magnetostatic Propagation for Uniform Normally Magnetized Multilayer Planar Structure," _AIP Conf. Proc._, Pittsburgh, PA, No. 34, pp. 280-282, June 1976.

38. Yukawa, T., Takeda, S., Abe, K. and Ikenoue, J-I., "Dispersion Surface of Magnetostatic Surface Waves Affected by Perfect Conductors," _IEEE Trans. on Magnetics_, vol. MAG-16, No. 5, pp. 687-689, September 1980.

39. Weinberg, I. J., "Dispersion Relations for Magnetostatic Waves," _1980 IEEE Ultrasonics Symp. Proc._, Boston, MA, pp. 557-561, November 1980.

40. Daniel, M. R., Adam, J. D. and O'Keeffe, T. W., "Linearly Dispersive Delay Lines at Microwave Frequencies Using Magnetostatic Waves," _1979 IEEE Ultrasonics Symp. Proc._, New Orleans, LA, pp. 806-809, September 1979.

41. Young, P., "Effect of Boundary Conditions on the Propagation of Surface Magnetostatic Waves in a Transversely Magnetized Thin YIG Slab," _Electronics Letters_, vol. 5, No. 18, pp. 429-431, September 1969.

42. Auld, B. A. and Mehta, K. B., "Magnetostatic Waves in a Transversely Magnetized Rectangular Rod," _J. Appl. Phys._, vol. 38, No. 10, pp. 4081-4082, September 1967.

43. Katz, H. W., _Solid State Magnetic and Dielectric Devices_, John Wiley and Sons, Inc., New York, pp. 268-274, 1959.

44. Lax, B. and Button, K. J., _Microwave Ferrites and Ferrimagnetics_, McGraw-Hill Book Co., Inc., New York, pp. 145-157, 1962.

45. Watkins, D. A., _Topics in Electromagnetic Theory_, John Wiley and Sons, Inc., New York, pp. 94-111, 1958.

46. Joseph, R. J. and Schlomann, E., "Demagnetizing Field in Non-ellipsoidal Bodies," _J. Appl. Phys._, vol. 36, No. 5, pp. 1579-1589, May 1965.

47. Sparks, M., _Ferromagnetic-Relaxation Theory_, McGraw-Hill Book Co., Inc., New York, pp. 14-16, 1964.

48. Lax, B. and Button, K. J., _Microwave Ferrites and Ferrimagnetics_, McGraw-Hill Book Co., Inc., New York, pp. 172-180, 1962.

49. Auld, B. A., "Walker Modes in Large Ferrite Samples," _J. Appl. Phys._, vol. 31, No. 9, pp. 1642-1647, September 1960.

50. Lax, B. and Button, K. J., <u>Microwave Ferrites and Ferrimagnetics</u>, McGraw-Hill Book Co., Inc., New York, pp. 297-322, 1962.

51. Seidel, H., "The Character of Waveguide Modes in Gyromagnetic Media," <u>Bell Sys. Tech. J.</u>, vol. 36, No. 2, pp. 409-426, March 1957.

52. Wolfe, R. and Kriessman, C. J., "Applied Solid State Science," Academic Press, Inc., New York, pp. 38-52, 1971.

53. Vasile, C. F. and LaRosa, R., "Guided Wave Propagation in Gyromagnetic Media as Applied to the Theory of Exchange Spin-Wave Excitation," <u>J. Appl. Phys.</u>, vol. 39, No. 3, pp. 1863-1872, February 1968.

54. Seidel, H. and Fletcher, R. C., "Gyromagnetic Modes in Waveguide Partially Loaded with Ferrite," <u>Bell Sys. Tech. J.</u>, vol. 38, No. 6, pp. 1427-1456, November 1959.

55. Adam, J. D. and Bajpai, S. N., "Magnetostatic Forward Volume Wave Propagation in YIG Strips," <u>IEEE Trans. on Magnetics</u>, vol. MAG-18, No. 6, pp. 1598-1600, November 1982.

56. Adams, J. D. and Collins, J. H., "Microwave Magnetostatic Delay Devices," <u>Proc. IEEE</u>, vol. 64, No. 5, pp. 794-801, May 1976.

57. Damon, R. W. and Van De Vaart, H., "Propagation of Magnetostatic Spin Waves at Microwave Frequences in a Normally Magnetized Disk," <u>J. Appl. Phys.</u>, vol. 36, No. 11, pp. 3453-3459, November 1965.

58. Vasile, C. F. and LaRosa, R., "Guided Wave Propagation in Gyromagnetic Media as Applied to the Theory of Exchange Spin-Wave Excitation," <u>J. Appl. Phys.</u>, vol. 39, No. 3, pp. 1863-1872, February 1968.

59. Bongiani, W. L., Collins, J. H., Pizzarello, F. A. and Hansen, W. W., "Propagating Magnetic Waves in Epitaxial YIG," <u>IEEE G-MTT Int. Microwave Symp. Digest of Tech. Papers</u>, Dallas, TX, pp. 376-380, May 1969.

60. Reimann, H., Hsia, L. C. and Wigen, P. E., "Magnetostatic Mode Spectra of Uniaxial Ferromagnets," <u>J. Appl. Phys.</u>, vol. 52, No. 3, pp. 2264-2267, March 1981.

61. O'Keeffe, T. W. and Patterson, R. W., "Magnetostatic Surface Wave Propagation in Finite Samples," <u>J. Appl. Phys.</u>, vol. 49, No. 9, pp. 4886-4895, September 1978.

62. Miller, N.D.J., "Non-reciprocal Magnetostatic Volume Waves," <u>IEEE Trans. on Magnetics</u>, vol. MAG-14, No. 5, pp. 829-831, September 1978.

63. Olson, F. A. and Yaeger, J. R., "Propagation, Dispersion and Attenuation of Backward-Travelling Magnetostatic Waves in YIG," *Appl. Phys. Letters*, vol. 5, No. 2, pp. 33-35, July 1964.

64. Miller, N.D.J., "Non-reciprocal Propagation of Magnetostatic Volume Waves," *Phys. Stat. Sol. (a)*, vol. 43, No. 2, pp. 593-600, October 1977.

65. Miller, N.D.J., "Magnetostatic Volume Wave Propagation in a Dielectric Layered Structure," *Phys. Stat. Sol. (a)*, vol. 37, No. 1, pp. 83-91, September 1976.

66. Bajpai, S. N. and Srivastava, B. J., "Magnetostatic Bulk Waves in an Arbitrary Magnetized YIG-Dielectric Layered Structure," *Phys. Stat. Sol. (a)*, vol. 57, No. 1, pp. 307-315, January 1980.

67. Stinson, D. C., "Intermediate Mathematics of Electromagnetics," Prentice Hall, Inc., Englewood Cliffs, NJ, pp. 121-143, 1976.

68. McCalla, T. R., "Introduction to Numerical Methods and FORTRAN Programming," John Wiley and Sons, Inc., New York, pp. 153-161, 1967.

69. McCalla, T. R., "Introduction to Numerical Methods and FORTRAN Programming," John Wiley and Sons, Inc., New York, pp. 82-90, 1967.

END

FILMED

3-85

DTIC